*Astronomy & Astrophysics* manuscript no. ms5
September 30, 2014
© ESO 2014

arXiv:1409.7906v1 [astro-ph.GA] 28 Sep 2014

# Near-infrared spectroscopy of candidate red supergiant stars in clusters. ⋆ ⋆⋆

Maria Messineo[1,2,3], Zhu Qingfeng[4], Valentin D. Ivanov[5], Donald F. Figer[3], Ben Davies[6], Karl M. Menten[1], Rolf P. Kudritzki[7], and C.-H. Rosie Chen[1]

[1] Max-Planck-Institut für Radioastronomie, Auf dem Hügel 69, D-53121 Bonn, Germany e-mail: messineo@mpifr-bonn.mpg.de
[2] European Space Agency (ESA), The Astrophysics and Fundamental Physics Missions Division, Research and Scientific Support Department, Directorate of Science and Robotic Exploration, ESTEC, Postbus 299, 2200 AG Noordwijk, The Netherlands
[3] Chester F. Carlson Center for Imaging Science, Rochester Institute of Technology, 54 Lomb Memorial Drive, Rochester, NY 14623-5604, United States
[4] Key Laboratory for Researches in Galaxies and Cosmology, University of Science and Technology of China, Chinese Academy of Sciences, Hefei, Anhui, 230026, China
[5] European Southern Observatory, Alonso de Cordoba 3107, Santiago, Chile
[6] Astrophysics Research Institute, Liverpool John Moores University, Twelve Quays House, Egerton Wharf, Birkenhead, Wirral. CH41 1LD, United Kingdom.
[7] Institute for Astronomy, University of Hawaii, 2680 Woodlawn Drive, Honolulu, HI 96822

Received September 15, 1996; accepted March 16, 1997

**ABSTRACT**

*Context.* Clear identifications of Galactic young stellar clusters farther than a few kpc from the Sun are rare, despite the large number of candidate clusters.
*Aims.* We aim to improve the selection of candidate clusters rich in massive stars with a multiwavelength analysis of photometric Galactic data that range from optical to mid-infrared wavelengths.
*Methods.* We present a photometric and spectroscopic analysis of five candidate stellar clusters, which were selected as overdensities with bright stars ($K_s < 7$ mag) in GLIMPSE and 2MASS images.
*Results.* A total of 48 infrared spectra were obtained. The combination of photometry and spectroscopy yielded six new red supergiant stars with masses from 10 $M_\odot$ to 15 $M_\odot$. Two red supergiants are located at Galactic coordinates (l,b)=(16.°7,−0.°63) and at a distance of about ∼ 3.9 kpc; four other red supergiants are members of a cluster at Galactic coordinates (l,b)=(49.°3,+0.°72) and at a distance of ∼ 7.0 kpc.
*Conclusions.* Spectroscopic analysis of the brightest stars of detected overdensities and studies of interstellar extinction along their line of sights are fundamental to distinguish regions of low extinction from actual stellar clusters. The census of young star clusters containing red supergiants is incomplete; in the existing all-sky near-infrared surveys, they can be identified as overdensities of bright stars with infrared color-magnitude diagrams characterized by gaps.

**Key words.** Stars: mass-loss, dust: extinction, Stars: supergiants, Stars: late-type, Galaxy: stellar content

## 1. Introduction

Stellar clusters are the best approximation in nature of a simple stellar population, they are the clocks of the Universe, and the building blocks of galaxies. More than 90% of massive stars are found in young and massive stellar clusters (de Wit et al. 2005).

In the inner regions of the Galactic disk, the identification of stellar clusters is a difficult task because of their irregular shapes and density profiles, and because of high and patchy interstellar extinction. About 3000 new candidate stellar clusters have been identified as significant peaks of stellar counts in the 2MASS and GLIMPSE catalogs, or with visual inspection of images (e.g., Borissova et al. 2011, 2014; Dutra et al. 2003; Froebrich et al. 2007; Ivanov et al. 2010; Mercer et al. 2005). However, only a few of these candidates have been confirmed with follow-up spectroscopic and photometric studies, mostly on the near-side of the Galactic plane (e.g., Chené et al. 2013; Davies et al. 2012; Messineo et al. 2009). A multiwavelength photometric screening/selection of candidate massive clusters is mandatory for the best use of the observing facilities, since spectroscopic follow-up can only be accessible for a limited number of candidate clusters. Typically, 50% of the detected overdensities are found to be spurious (Froebrich et al. 2007). For example, overdensities may result from regions of low interstellar extinction (e.g., Dutra et al. 2002). An overdensity can be defined as a cluster of stars if it is made of stars at the same distance and approximately the same age. Depending on the dynamical status, a cluster can be a bound cluster or an association. Typically, cluster members have similar interstellar extinction, and may be recognized on color magnitude diagrams (CMDs) as specific sequences.

A new class of stellar clusters has recently been discovered, the red supergiant clusters (RSGCs), which are characterized by a large number of red supergiants (RSGs) (Clark et al. 2009; Davies et al. 2007; Figer et al. 2006; González-Fernández & Negueruela 2012; Negueruela et al.

⋆ Based on observations collected at the European Southern Observatory (ESO Programme 60.A-9700(E), and 089.D-0876, and on observations collected at the UKIRT telescope (programme ID H243NS).

⋆⋆ MM is currently employed by the MPIfR. Part of this work was performed at RIT (2009), at ESA (2010), and at the MPIfR.

**Table 1.** List of candidate cluster positions, apparent radii, $<A_{K_s}>$, and modulus distances (DM).

| ID | RA(J2000)[a] [hh mm ss] | DEC(J2000)[a] [° ′ ″] | radius [″] | $< A_{K_s\ field} >$[b] [mag] | DM($< A_{K_s\ field} >$)[c] [mag] | $< A_{K_s\ cRSGs} >$[d] [mag] | DM($< A_{K_s\ RSGs} >$)[e] [mag] | DM(red clump)[f] [mag] | DM(Sp)[g] [mag] |
|---|---|---|---|---|---|---|---|---|---|
| cl1.5 | 17 53 45.09 | -28 11 08.29 | 73 | 0.45 ± 0.08 | (12.7 ± 0.2) | ··· | ··· | 14.54 ± 0.16 | ··· |
| cl9.5 | 18 10 54.34 | -21 12 37.67 | 60 | 0.70 ± 0.11 | (13.3 ± 0.2) | ··· | ··· | 14.05 ± 0.12 | ··· |
| cl16.7 | 18 23 34.40 | -14 39 10.86 | 76 | 0.44 ± 0.27 | 12.7 ± 0.9 | 0.49 ± 0.03 | 12.8 ± 0.1 | 12.93 ± 0.13 | ··· |
| cl49.3 | 19 19 31.53 | 14 54 08.57 | 130 | 0.48 ± 0.35 | 13.8 ± 1.9 | 0.47 ± 0.11 | 13.7 ± 0.5 | 14.22 ± 0.12 | 14.16 ± 1.00 |
| cl59.8 | 19 46 18.57 | 23 22 30.23 | 85 | 0.26 ± 0.17 | 12.9 ± 1.4 | ··· | ··· | ··· | ··· |

**Notes:** (*a*) Positions are derived as the centroid of surface brightness maps from 2MASS $K_s$ band images. (*b*) $< A_{K_s\ field} >$ is the average $A_{K_s}$ of the spectroscopically observed late-type stars in the field. (*c*) DM($< A_{K_s\ field} >$) is the distance modulus obtained from the $A_{K_s}$ values of detected late-type stars and the model of Drimmel et al. (2003). (*d*) $< A_{K_s\ RSGs} >$ is the average $A_{K_s}$ of the detected RSGs. (*e*) DM($< A_{K_s\ RSGs} >$) is the distance modulus obtained from the $A_{K_s}$ values of cRSGs and the model of Drimmel et al. (2003). (*f*) DM(red clump) is the distance modulus obtained from the $A_{K_s}$ values of cRSGs and field red clump stars. (*g*) DM(Sp): spectro-photometric distance modulus of star 39, by assuming a giant case (O9.5-B3III). For a dwarf case, DM would be 13.02 ± 0.77 mag.

2011, 2010). RSGC1, RSGC2, RSGC3, RSGC4, and RSGC5 contain 14, 26, ∼ 35, > 13, and 7 RSGs, respectively, or collectively ∼15% of all known RSGs in the Galaxy (Messineo et al. 2012). These newly discovered RSGCs are all concentrated between longitude $l = 25°$ and $l = 30°$, i.e., close to the near end of the Galactic bar, where the bar appears to meet the Scutum-Crux spiral arm. However, their census is incomplete (e.g., Messineo et al. 2012); further searches for RSGCs are needed to investigate Galactic structure. RSGCs are dominated by RSGs, which are intrinsically bright at infrared wavelengths. Their near-infrared CMDs are characterized by gaps of several magnitudes between the RSGs and the blue supergiant members. RSGCs are detected as overdensities of solely infrared bright stars, so bright (typically $K_s \lesssim 7.0$ mag at 6 kpc) that they can be detected throughout the Galactic plane; infrared dimmer main sequence members are hard to identify in the glare of bright RSGs.

In this paper, we analyze five candidate clusters rich in infrared bright stars that show different types of CMDs by means of a quantitative analysis of near-infrared spectra of their brightest stars. In Sect. 2, we describe the observed candidate stellar clusters; in Sect. 3, we report on the available infrared spectroscopic and photometric data. Spectral and photometric classifications are given in Sect. 4. The cluster properties are discussed in Sect. 6. Finally, our findings are summarized in Sect. 7.

## 2. Targeted candidate clusters

A random sample of candidate stellar clusters were selected among overdensities of infrared-bright stars in both GLIMPSE and 2MASS images (see, e.g., Ivanov et al. 2002, 2010). The candidate clusters were selected to have different types of CMDs, with gaps and without gaps (see Sect. 6). The observed candidate clusters are listed in Table 1. The list reports their coordinates, which are the flux weighted centroids of 5′×5′ $K_s$ band images from 2MASS. The overdensities of infrared-bright stars are shown in Fig. 1, and in the star counts of Table 2.

## 3. Data

### *3.1. Near-IR spectroscopy*

#### 3.1.1. UIST spectra

A set of spectroscopic data was taken with the UKIRT 1-5 micron Imager Spectrometer (UIST; Ramsay Howat et al. 1998) on Mauna Kea under program ID H243NS (PI: Kudritzki) on 2008 July 24. We used the long-K grism, which covers from 2.204 $\mu$m to 2.513 $\mu$m at a resolving power (R) of 1900. Integration times varied from 10 s to 45 s per exposure, and the number of exposures varied from 8 to 20.

**Table 2.** Counts of stars with $K_s$> 10.0, 8.5, and 7.0 mag in the fields listed in Table 1, and, as a comparison, in control fields of equal area.

| ID | Center/Control fields | | |
|---|---|---|---|
| | Nstar ( $K_s$ < 10 mag) | Nstar ($K_s$ < 8.5 mag) | Nstar ($K_s$ < 7 mag) |
| cl1.5 | 57/24 | 8/1 | 1/1 |
| cl9.5 | 21/06 | 4/1 | 1/1 |
| cl16.7 | 15/09 | 7/2 | 4/1 |
| cl49.3 | 27/14 | 7/5 | 5/1 |
| cl59.8 | 9/02 | 5/1 | 3/1 |

Pairs of adjacent frames at different nod-positions were subtracted from each other and flat-fielded, wavelength-calibrated with Ar arc lines, and corrected for atmospheric absorption and instrumental response. Curves of atmospheric absorption and instrumental response were generated by dividing the observed spectra of standard stars (with spectral types from B2 to B9) by blackbody curves. Linear interpolation was used to remove Br$\gamma$ lines and possible He I lines from the spectra of the standards. A total of 22 stars were observed with UKIRT, and are listed in Tables 3 and 4; their spectra are shown in Fig. 2.

#### 3.1.2. SOFI spectra

For four of the targeted candidate clusters, additional low-resolution and medium-resolution spectra were obtained with the SofI spectrograph mounted on the NTT telescope (Moorwood et al. 1998). Data were taken under program 60.A-9700(E) at Paranal-La Silla Observatory on 2010 August 3, and under program 089.D-0876 on 2012 June 1. The pixel scale is 0.″288 pix$^{-1}$. The low-resolution Red grism in combination with the 0.″6 × 290″ slit yielded R ≈980 over the range ∼1.50 $\mu$m to ∼2.49 $\mu$m. A few spectra were taken with the HR grism, the $K_s$ filter, and a 1.″0-wide slit (R ≈ 1900).

Typically, two slit positions per cluster were observed. The rotator angle was set to optimize the number of stars falling onto the slit. For each slit, frames were taken in a nodding sequence ABBA, which included a small jittering between positions, with detector integration times (DITs) from 1.18 s to 120 s. B-type stars were selected as standards, and observed with the same settings as the targets.

Data reduction was carried out with IDL programs, and the Image Reduction and Analysis Facility (IRAF), using the

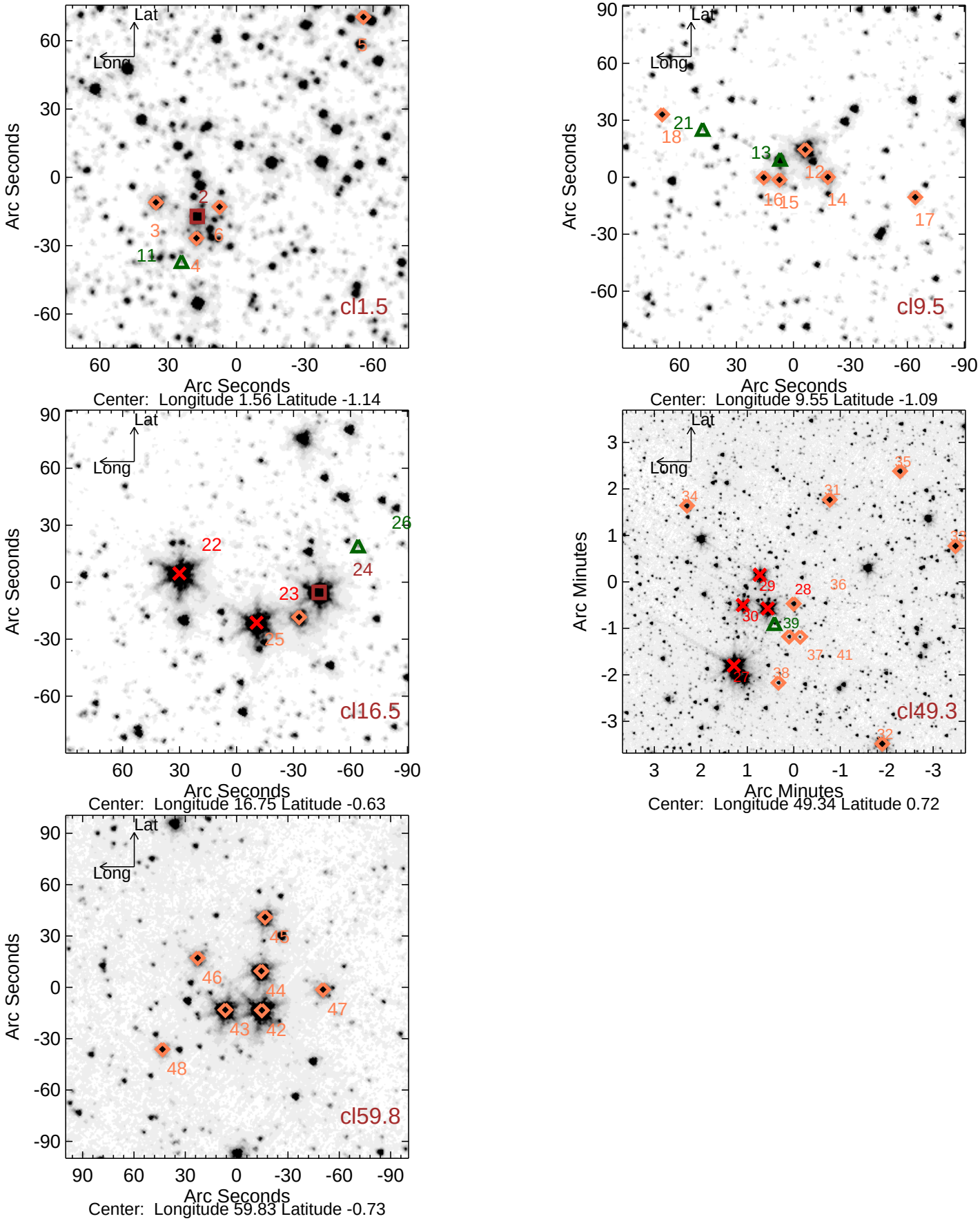


**Fig. 1.** GLIMPSE 3.6 $\mu$m images of the candidate clusters listed in Table 1: cl1.5, cl9.5, cl16.5, cl49.3, and cl59.8. Spectroscopic targets are labeled as in Tables 3 and 4. Diamonds indicate red giants, squares Mira-like AGB stars, crosses RSG stars, and triangles early- and yellow-type stars. The coordinates of the image centers are in degrees.

**Table 3.** Infrared counterparts of the spectroscopically observed targets.

| | | | 2MASS | | | DENIS | | | GLIMPSE | | | | MSX[a] | | | | WISE[b] | | | | NOMAD | | |
|---|---|---|---|---|---|---|---|---|---|---|---|---|---|---|---|---|---|---|---|---|---|---|---|
| ID | RA(J2000) | DEC(J2000) | *J* | *H* | $K_S$ | *I* | *J* | $K_S$ | [3.6] | [4.5] | [5.8] | [8.0] | *A* | *D* | *C* | *D* | *W1* | *W2* | *W3* | *W4* | *B* | *V* | *R* |
| | [hh mm ss] | [deg mm ss] | [mag] | [mag] | [mag] | [mag] | [mag] | [mag] | [mag] | [mag] | [mag] | [mag] | [mag] | [mag] | [mag] | [mag] | [mag] | [mag] | [mag] | [mag] | [mag] | [mag] | [mag] |
| 1 | 17 53 60.00 | -28 10 50.19 | 7.48 | 5.88 | 4.86 | ··· | ··· | ··· | ··· | ··· | ··· | ··· | 1.56 | 0.67 | 0.70 | 0.01 | ··· | ··· | ··· | ··· | ··· | ··· | ··· |
| 2 | 17 53 45.50 | -28 11 07.12 | 9.68 | 8.17 | 7.35 | ··· | ··· | ··· | 6.94 | 7.00 | 6.69 | 6.46 | 5.88 | ··· | ··· | ··· | 6.74 | 6.72 | 5.72 | 4.78 | ··· | ··· | ··· |
| 3 | 17 53 45.80 | -28 10 48.35 | 10.57 | 8.91 | 8.09 | ··· | ··· | ··· | 7.45 | 7.55 | 7.20 | 7.08 | ··· | ··· | ··· | ··· | 7.69 | 7.41 | 6.73 | 6.11 | ··· | ··· | ··· |
| 4 | 17 53 46.14 | -28 11 11.64 | 10.57 | 9.20 | 8.54 | ··· | ··· | ··· | 8.18 | 8.28 | 8.06 | 8.01 | ··· | ··· | ··· | ··· | ··· | ··· | ··· | ··· | 17.89 | ··· | 17.41 |
| 5 | 17 53 36.99 | -28 11 25.62 | 10.84 | 9.43 | 8.81 | ··· | ··· | ··· | 8.52 | 8.72 | 8.51 | 8.48 | ··· | ··· | ··· | ··· | 7.83 | 7.80 | 8.10 | ··· | ··· | ··· | 18.65 |
| 6 | 17 53 44.85 | -28 11 13.42 | 11.07 | 9.57 | 9.01 | ··· | ··· | ··· | 8.69 | 8.80 | 8.65 | 8.63 | ··· | ··· | ··· | ··· | ··· | ··· | ··· | ··· | ··· | ··· | 19.54 |
| 7 | 17 53 58.30 | -28 10 54.96 | 10.95 | 9.67 | 9.07 | ··· | ··· | ··· | 8.80 | 8.84 | 8.59 | 8.73 | ··· | ··· | ··· | ··· | 8.86 | 9.18 | ··· | ··· | ··· | 13.15 | ··· |
| 8 | 17 54 03.84 | -28 10 46.62 | ··· | 10.71 | 10.06 | ··· | ··· | ··· | 9.68 | 9.77 | 9.42 | 9.47 | ··· | ··· | ··· | ··· | 9.64 | 9.74 | ··· | 6.40 | 18.81 | ··· | 23.26 |
| 9 | 17 53 35.93 | -28 11 25.89 | 11.00 | 10.30 | 10.08 | ··· | ··· | ··· | 10.02 | 10.06 | 10.00 | 9.99 | ··· | ··· | ··· | ··· | ··· | ··· | ··· | ··· | 14.39 | 13.28 | 13.24 |
| 10 | 17 54 01.74 | -28 10 49.68 | 12.15 | 10.78 | 10.23 | ··· | ··· | ··· | 9.89 | 10.04 | 9.53 | 9.67 | ··· | ··· | ··· | ··· | ··· | ··· | ··· | ··· | 17.28 | 16.42 | ··· |
| 11 | 17 53 47.05 | -28 11 11.16 | 12.48 | 12.28 | 12.24 | ··· | ··· | ··· | 12.10 | 12.18 | 12.16 | 12.15 | ··· | ··· | ··· | ··· | ··· | ··· | ··· | ··· | 13.37 | 12.75 | 13.10 |
| 12 | 18 10 53.31 | -21 12 34.75 | 8.93 | 7.18 | 6.39 | 14.69 | 9.33 | 6.84 | 6.35 | 6.04 | 5.75 | 5.54 | 5.15 | ··· | ··· | ··· | 5.54 | 5.80 | 4.89 | 3.81 | ··· | ··· | ··· |
| 13 | 18 10 54.09 | -21 12 25.57 | 7.99 | 7.96 | 7.83 | 9.03 | 8.52 | 8.28 | 7.78 | 7.79 | 7.74 | 7.80 | ··· | ··· | ··· | ··· | 7.72 | 7.71 | 7.63 | 7.82 | 9.01 | 8.79 | 8.66 |
| 14 | 18 10 53.81 | -21 12 52.15 | 10.74 | 8.90 | 8.02 | 17.59 | 11.14 | 8.54 | 7.48 | 7.61 | 7.31 | 7.27 | ··· | ··· | ··· | ··· | 7.56 | 7.48 | 6.87 | 5.65 | ··· | ··· | ··· |
| 15 | 18 10 54.78 | -21 12 30.55 | 10.91 | 9.05 | 8.13 | ··· | 10.80 | 8.05 | 7.51 | 7.79 | 7.41 | 7.31 | ··· | ··· | ··· | ··· | 7.74 | 7.71 | 6.96 | 6.00 | ··· | ··· | ··· |
| 16 | 18 10 54.99 | -21 12 22.67 | 11.44 | 9.63 | 8.84 | 16.16 | 11.72 | 9.23 | 8.20 | 8.12 | 7.91 | 7.79 | ··· | ··· | ··· | ··· | 8.40 | 8.19 | 7.89 | 7.51 | ··· | ··· | ··· |
| 17 | 18 10 52.89 | -21 13 37.62 | 11.96 | 10.34 | 9.49 | 16.77 | 12.43 | 9.79 | ··· | ··· | ··· | ··· | ··· | ··· | ··· | ··· | ··· | ··· | ··· | ··· | ··· | ··· | ··· |
| 18 | 18 10 54.75 | -21 11 19.81 | 11.73 | 10.18 | 9.60 | 15.89 | 12.01 | 9.88 | 9.30 | 9.40 | 9.13 | 9.15 | ··· | ··· | ··· | ··· | 9.19 | 9.27 | 8.69 | 7.14 | ··· | ··· | 18.08 |
| 19 | 18 10 54.82 | -21 10 49.14 | 12.05 | 11.88 | 11.76 | 12.92 | 12.63 | 12.31 | 11.66 | 11.51 | 11.65 | 12.02 | ··· | ··· | ··· | ··· | ··· | ··· | ··· | ··· | 12.97 | 12.87 | 11.95 |
| 20 | 18 10 55.33 | -21 10 15.97 | 12.38 | 12.02 | 11.77 | 13.41 | 13.06 | 12.02 | 11.55 | 11.50 | 11.58 | 11.59 | ··· | ··· | ··· | ··· | ··· | ··· | ··· | ··· | 13.90 | 13.64 | 13.33 |
| 21 | 18 10 54.50 | -21 11 42.23 | 14.22 | 12.96 | 12.49 | ··· | 14.83 | 13.06 | 12.11 | 12.11 | 11.88 | 12.57 | ··· | ··· | ··· | ··· | ··· | ··· | ··· | ··· | ··· | ··· | ··· |
| 22 | 18 23 35.07 | -14 38 40.87 | 6.38 | 5.15 | 4.55 | 9.41 | 6.22 | 3.97 | ··· | ··· | 4.21 | 4.23 | 4.07 | ··· | ··· | ··· | 4.27 | 4.15 | 4.21 | 4.00 | 15.40 | 13.70 | 12.21 |
| 23 | 18 23 35.33 | -14 39 28.95 | 7.01 | 5.68 | 5.06 | 11.25 | 6.78 | 4.22 | 4.65 | 4.75 | 4.35 | 4.18 | 4.02 | 3.18 | 3.02 | ··· | 4.75 | 4.14 | 3.66 | 2.60 | 18.98 | 16.47 | 15.04 |
| 24 | 18 23 33.30 | -14 39 50.57 | 9.74 | 7.34 | 5.91 | 13.77 | 8.93 | 4.80 | ··· | ··· | 4.07 | 3.72 | 2.96 | 1.97 | 1.88 | 1.58 | 4.56 | 3.30 | 2.43 | 1.32 | 16.09 | 15.33 | 13.40 |
| 25 | 18 23 34.43 | -14 39 47.33 | 9.11 | 7.43 | 6.64 | 13.64 | 9.03 | 6.46 | 6.71 | 6.34 | 6.08 | 6.09 | ··· | ··· | ··· | ··· | 6.15 | 6.41 | 6.45 | 6.45 | ··· | ··· | ··· |
| 26 | 18 23 31.14 | -14 39 57.17 | 13.12 | 12.52 | 12.10 | 14.55 | 13.00 | 11.89 | 11.86 | 11.92 | 11.60 | ··· | ··· | ··· | ··· | ··· | ··· | ··· | ··· | ··· | 16.20 | 15.36 | 15.00 |
| 27 | 19 19 33.81 | 14 53 55.68 | 5.49 | 4.52 | 4.12 | ··· | ··· | ··· | 3.83 | 3.91 | 3.60 | 3.37 | 3.10 | 2.61 | 2.67 | 1.41 | 3.69 | 3.39 | 2.90 | 2.06 | 14.55 | 17.18 | 10.84 |
| 28 | 19 19 27.91 | 14 53 51.64 | 7.40 | 5.98 | 5.41 | ··· | ··· | ··· | 4.89 | 5.31 | 4.92 | 4.72 | 4.57 | ··· | ··· | ··· | 5.04 | 4.93 | 4.53 | 3.76 | ··· | 15.00 | ··· |
| 29 | 19 19 25.58 | 14 54 21.07 | 7.88 | 6.54 | 5.97 | ··· | ··· | ··· | ··· | 5.91 | 5.57 | 5.46 | 5.49 | ··· | ··· | ··· | 5.62 | 5.69 | 5.44 | 4.83 | 16.92 | 15.09 | 12.95 |
| 30 | 19 19 28.68 | 14 54 21.98 | 8.41 | 6.93 | 6.38 | ··· | ··· | ··· | 5.72 | 6.23 | 5.96 | 5.93 | ··· | ··· | ··· | ··· | 5.99 | 6.11 | 5.97 | 5.58 | 16.67 | 15.07 | 13.25 |
| 31 | 19 19 16.76 | 14 53 46.72 | 8.35 | 7.49 | 7.16 | ··· | ··· | ··· | 6.97 | 7.16 | 7.00 | 6.97 | ··· | ··· | ··· | ··· | 6.93 | 7.08 | 7.06 | 7.31 | 14.17 | 12.82 | 10.74 |
| 32 | 19 19 33.77 | 14 50 19.19 | 10.18 | 8.48 | 7.40 | ··· | ··· | ··· | 6.12 | 5.99 | 5.63 | 5.29 | 5.22 | ··· | ··· | ··· | 6.31 | 5.76 | 4.62 | 3.79 | 13.72 | 13.08 | 12.01 |
| 33 | 19 19 15.15 | 14 50 55.29 | 11.09 | 9.11 | 7.93 | ··· | ··· | ··· | 6.79 | 6.65 | 6.22 | 5.89 | 5.46 | ··· | ··· | ··· | 6.52 | 5.98 | 4.65 | 3.74 | ··· | ··· | ··· |
| 34 | 19 19 23.18 | 14 56 26.01 | 9.14 | 8.35 | 8.06 | ··· | ··· | ··· | 7.93 | 8.10 | 7.95 | 7.87 | ··· | ··· | ··· | ··· | 7.61 | 7.84 | 7.89 | 8.64 | 14.22 | 13.18 | 10.74 |
| 35 | 19 19 11.58 | 14 52 43.78 | 8.86 | 8.28 | 8.09 | ··· | ··· | ··· | 8.02 | 8.08 | 7.96 | 7.96 | ··· | ··· | ··· | ··· | 7.97 | 8.02 | 7.98 | 8.45 | 12.51 | 11.52 | 10.92 |
| 36 | 19 19 26.44 | 14 53 25.01 | 10.19 | 8.86 | 8.39 | ··· | ··· | ··· | 8.06 | 8.23 | 8.04 | 8.01 | ··· | ··· | ··· | ··· | 8.05 | 8.17 | 8.28 | ··· | ··· | ··· | ··· |
| 37 | 19 19 29.23 | 14 53 10.32 | 12.00 | 10.60 | 10.07 | ··· | ··· | ··· | 9.74 | 9.88 | 9.69 | 9.65 | ··· | ··· | ··· | ··· | 9.76 | 9.86 | 10.38 | 8.52 | ··· | ··· | ··· |
| 38 | 19 19 33.30 | 14 52 54.58 | 12.76 | 11.01 | 10.24 | ··· | ··· | ··· | 9.87 | 10.00 | 9.74 | 9.74 | ··· | ··· | ··· | ··· | 9.91 | 9.99 | ··· | ··· | ··· | ··· | 20.68 |
| 39 | 19 19 28.80 | 14 53 35.01 | 12.10 | 11.50 | 11.19 | ··· | ··· | ··· | 10.94 | 10.97 | 10.79 | 10.93 | ··· | ··· | ··· | ··· | ··· | ··· | ··· | ··· | 17.47 | ··· | 13.82 |
| 40 | 19 19 15.15 | 14 49 54.25 | 13.55 | 11.99 | 11.29 | ··· | ··· | ··· | ··· | ··· | ··· | ··· | ··· | ··· | ··· | ··· | ··· | ··· | ··· | ··· | ··· | 17.92 | ··· |
| 41[c] | 19 19 28.78 | 14 52 57.50 | 12.56 | 11.76 | 11.48 | ··· | ··· | ··· | ··· | ··· | ··· | ··· | ··· | ··· | ··· | ··· | ··· | ··· | ··· | ··· | 17.22 | ··· | 14.07 |
| 42 | 19 46 18.93 | 23 22 10.72 | 8.95 | 7.32 | 6.49 | ··· | ··· | ··· | 6.01 | 6.01 | 5.68 | 5.49 | 5.25 | ··· | ··· | ··· | 6.02 | 5.82 | 5.07 | 4.14 | ··· | ··· | 19.86 |
| 43 | 19 46 19.70 | 23 22 29.28 | 8.58 | 7.29 | 6.73 | ··· | ··· | ··· | 6.39 | 6.67 | 6.40 | 6.37 | ··· | ··· | ··· | ··· | 6.43 | 6.57 | 6.41 | 6.18 | 18.16 | 16.02 | 14.31 |
| 44 | 19 46 17.50 | 23 22 22.46 | 8.05 | 7.24 | 6.97 | ··· | ··· | ··· | 6.85 | 7.01 | 6.90 | 6.82 | ··· | ··· | ··· | ··· | 6.80 | 6.94 | 6.86 | 6.54 | 14.46 | 11.40 | 11.58 |
| 45 | 19 46 15.45 | 23 22 36.41 | 11.10 | 9.13 | 8.22 | ··· | ··· | ··· | 7.47 | 7.51 | 7.17 | 7.03 | 6.74 | ··· | ··· | ··· | 7.47 | 7.21 | 6.48 | 5.40 | ··· | ··· | ··· |
| 46 | 19 46 18.38 | 23 22 58.52 | 10.24 | 8.86 | 8.39 | ··· | ··· | ··· | 8.14 | 8.30 | 8.09 | 8.03 | ··· | ··· | ··· | ··· | 8.13 | 8.20 | 8.06 | 7.27 | 18.44 | 16.72 | 15.43 |
| 47 | 19 46 16.87 | 23 21 45.87 | 9.63 | 8.75 | 8.54 | ··· | ··· | ··· | 8.44 | 8.52 | 8.46 | 8.42 | ··· | ··· | ··· | ··· | 8.37 | 8.45 | 8.46 | 7.90 | 14.24 | 12.96 | 12.04 |
| 48 | 19 46 22.48 | 23 22 49.50 | 10.67 | 9.45 | 9.03 | ··· | ··· | ··· | 8.80 | 8.97 | 8.76 | 8.74 | ··· | ··· | ··· | ··· | 8.73 | 8.80 | 8.74 | 7.57 | 18.29 | 16.65 | 15.32 |

**Notes:** ([a]) Upper-limit magnitudes were removed. ([b]) Measurements with signal-to-noise ratio smaller than 2 were removed. ([c]) For star 41, the adopted *J*, *H*, and *K* measurements are from the UKIDSS survey.

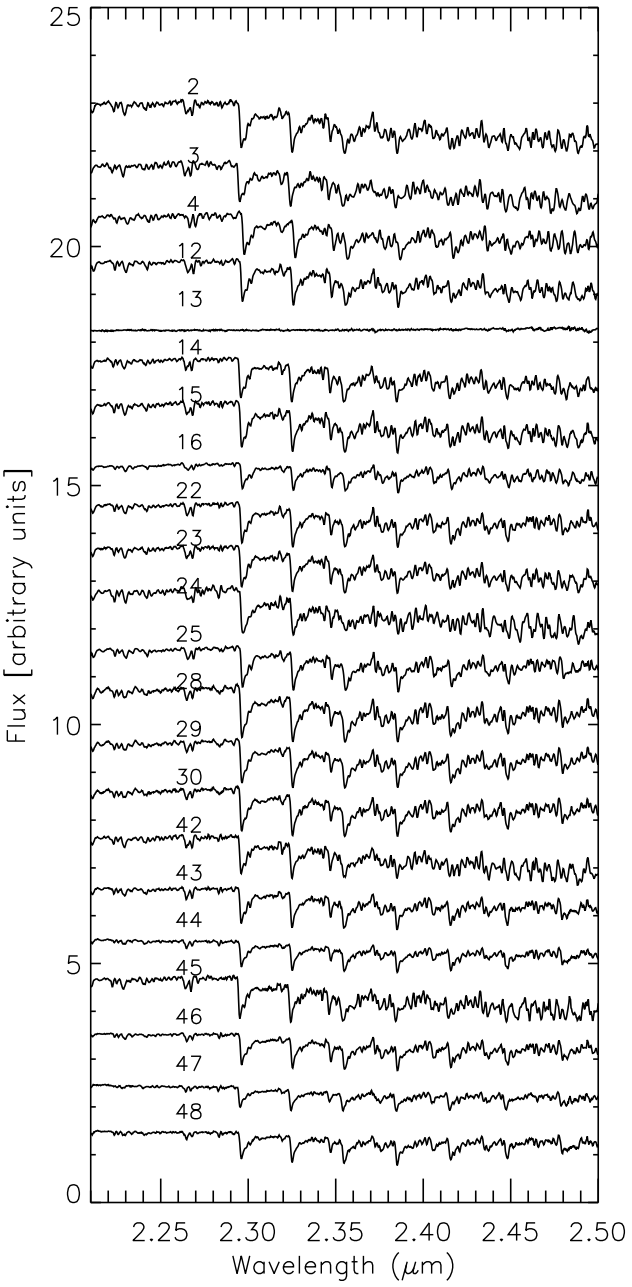


**Fig. 2.** Long-*K* spectra taken with UIST. Identification numbers refer to Table 4. All are late-type stars, with the exception of star 13.

NOAO/onedspec package[1]. Pairs of subsequent images at different nod-positions were subtracted and flat-fielded. Wavelength calibration was performed with observations of arc lamps. Only spectra with a signal-to-noise ratio above 30 were used. For each star, typically, four spectra were combined and then corrected for atmospheric transmission and instrumental response. Hydrogen and helium lines were removed from the spectra of the standard stars with a linear interpolation; the intrinsic continuum slopes of the standard spectra were eliminated by dividing them by blackbody curves (calculated at the $T_{\rm eff}$ of the standard stars). A total of 28 low-resolution spectra and 13 medium-resolution spectra were obtained (see Table 4, Fig. 3, and Fig. 4).

[1] IRAF is distributed by the National Optical Astronomy Observatories, which is operated by the Association of Universities for Research in Astronomy, Inc., under cooperative agreement with the National Science Foundation.

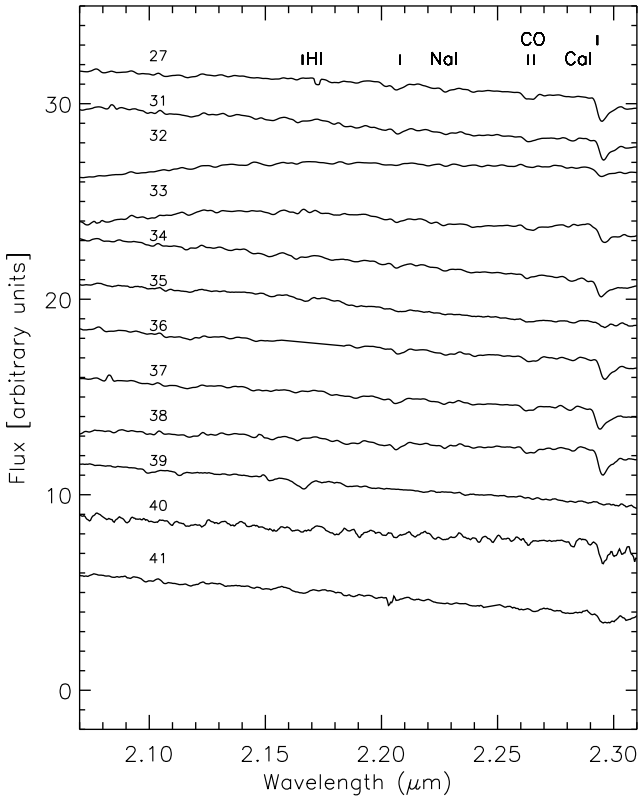


**Fig. 4.** Medium-resolution *K* spectra taken with SofI. Identification numbers are taken from Table 4. All stars are late-type stars, with the exception of star 39.

### 3.2. Photometric data

For the target stars, simultaneous photometric measurements in bands *J*, *H*, and $K_{\rm s}$ were available in the Two Micron all Sky Survey (2MASS) catalog (Skrutskie et al. 2006), with 1.″0 resolution; for two fields, additional near-infrared measurements (simultaneous *I*, *J*, and $K_{\rm s}$) were available from the Deep Near-Infrared Survey (DENIS) catalog (Epchtein et al. 1999). Deep *J*, *H*, and *K* photometry was obtained from the UKIDSS Galactic Plane Survey (Hodgkin et al. 2009; Lucas et al. 2008).

Mid-infrared data were available from the Galactic Legacy Infrared Mid–Plane Survey Extraordinaire (GLIMPSE) with the Spitzer Space Telescope, from the Midcourse Space Experiment (MSX) Spatial Infrared Imaging Telescope (SPIRIT III), and from the Wide-field Infrared Survey Explorer (WISE) satellite (Benjamin et al. 2003; Egan et al. 2003; Fazio et al. 2004; Wright et al. 2010). The SPITZER/IRAC camera acquired simultaneous images in the four channels at 3.6, 4.5, 5.8, and 8.0 $\mu$m, with a spatial resolution of 1.″2 and a sensitivity of 2 mJy. MSX covered from 8 $\mu$m to 21 $\mu$m, with a pixel scale of 18.″3, and a sensitivity of 0.1 Jy at the short-wavelength. WISE bands are centered at 3.4, 4.6, 12, and 22 $\mu$m; detectability limits are 0.08, 0.11, 1, and 6 mJy; spatial resolutions are 6.″1, 6.″4, 6.″5, and 12.″0, respectively.

DENIS and 2MASS data were cross-matched using a search radius of 2.″0; 2MASS astrometry was retained. Mid-infrared

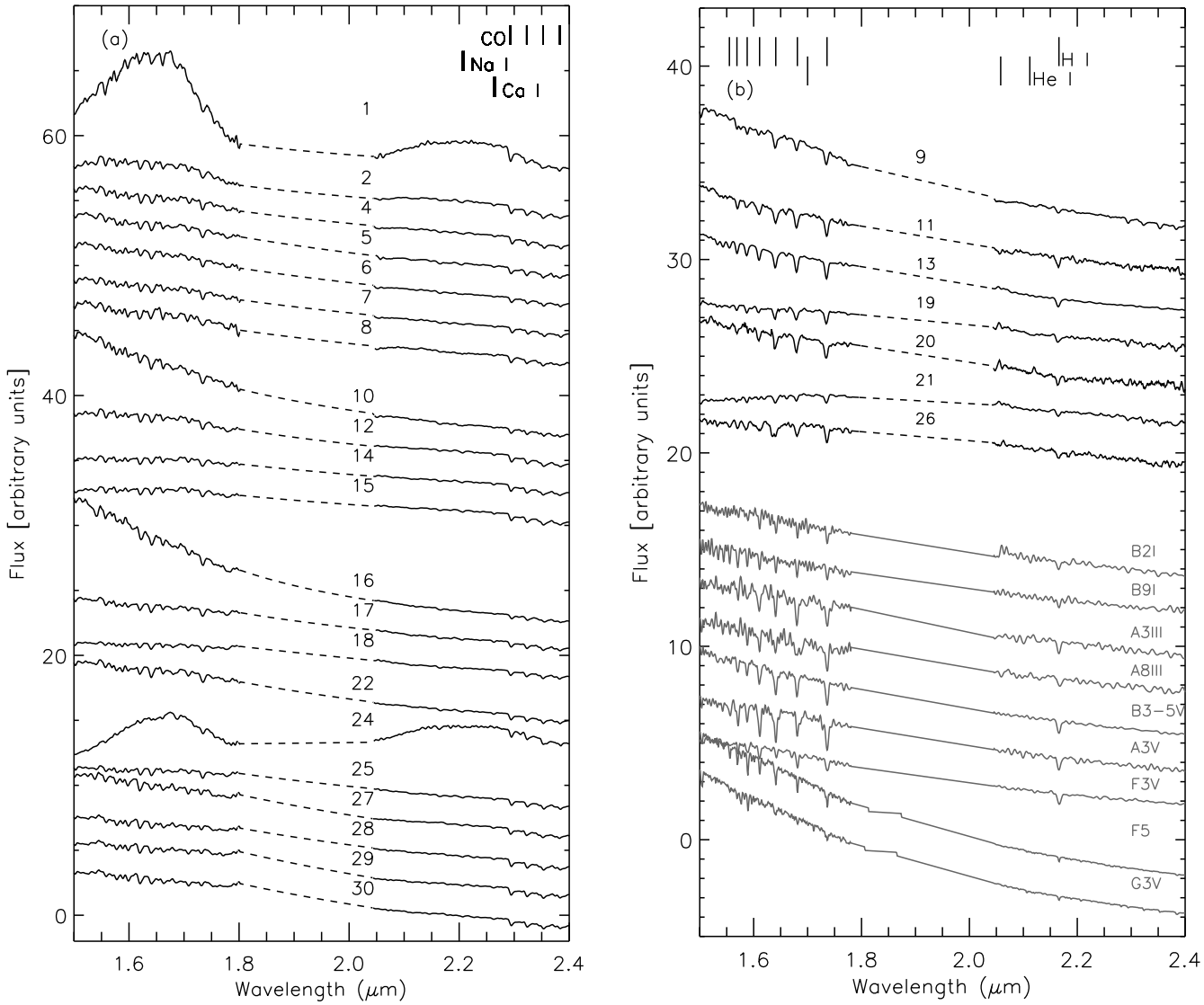


**Fig. 3.** Low-resolution *H* and *K* spectra taken with SofI. Identification numbers are taken from Table 4. Late-type stars are shown in panel *(a)*. Early-type stars are shown in panel *(b)* together with a few low-resolution template spectra from the library of Lancon & Rocca-Volmerange (1992), and medium-resolution template spectra from the IRTF library (Rayner et al. 2009).

counterparts from the MSX catalog were searched within a radius of 5″; matches from the WISE and GLIMPSE catalogs within a radius of 2″. In addition, we checked for possible visual counterparts in the NOMAD catalog of Zacharias et al. (2004), using a search radius of 2″.

Photometric measurements of the spectroscopic targets are listed in Table 3.

### 3.2.1. UKIDSS photometry

We used JHK photometry from the UKIDSS Galactic Plane Survey (GPS). For every position, JHK images were obtained from the UKIDSS archive. Raw frames were processed by the standard UKIDSS pipeline (Lucas et al. 2008); corrections for linearity, dark, flat-fielding, decurtaining (the removal of a pseudo-periodic ripple), defringing (the removal of interference fringes due to atmospheric emission lines), sky-subtraction, and cross-talk were applied.

The original WFCAM pixel scale is of 0.″4 pix$^{-1}$; however, GPS observations were performed with a $2 \times 2$ micro-stepping technique, which improved the sampling; a microstep of 11.5 pixels was used. Each observation comprises eight individual exposures of duration 10, 10, and 5 s to make up integration times on sources of 80, 80, and 40 s in the *J*, *H*, and *K* filters, respectively. We resampled the exposures of each observation in a finer grid ($3 \times 3$) in order to reduce the image noise, and to improve the detectability of faint sources; we used a bilinear interpolation. Exposures were combined with a three $\sigma$ clipping to eliminate possible cosmic rays. The astrometric distortion of the final mosaic was corrected by using a set of unsaturated stars with 2MASS photometry, and performing a polynomial spatial de-warping of third order. Source extraction was performed using the DAOPHOT PSF-fitting algorithm by Stetson (1987). For each mosaic, a set of bright and isolated unsaturated stars were selected, and a invariable PSF was modeled. The detection threshold was set to 4 $\sigma$ (the standard deviation). Finally, individual *J*, *H*, and *K* catalogs were photometrically calibrated with

overlapping 2MASS sources, positionally cross-correlated, and combined.

For saturated stars that could be uniquely associated with a 2MASS point source, 2MASS magnitudes were retained.

### 3.3. Information available on SIMBAD

The SIMBAD database reports information only for one target. We classified star 13 as a B0-F0 star; the star coincides with HD166307, which has been classified as an A0III star at optical wavelength (Houk & Smith-Moore 1988).

## 4. Stellar classification

We detected candidate RSGs in two fields. In order to confirm RSGs in the direction of the inner disk of the Milky Way, a complex procedure is required. Spectroscopic observations alone cannot firmly distinguish between RSGs and red giant stars. When analyzing RSGs, it is crucial to combine spectroscopic information (see Sect. 4.1) with photometric quantities (see Sects. 4.1.3 and 4.1.4), and to estimate their fundamental parameters (effective temperatures, $T_{\rm eff}$, and luminosities). Distances of late-type stars are usually estimated in two ways, either approximated with kinematic distances, or estimated using interstellar extinction as an indicator of distance (e.g., Drimmel et al. 2003; Habing et al. 2006; Messineo et al. 2005). In the inner Galaxy kinematic distances alone cannot be trusted as they rely on the assumption of circular orbits that is not valid in the inner 3.5 kpc (e.g., de Vaucouleurs 1964); our estimates of distances are based on interstellar extinction (Sect. 4.2). Luminosities are described in Sect. 4.3.

### 4.1. Spectroscopic classification

#### 4.1.1. Late-type stars

We defined as late-type stars those stars with effective temperatures lower than 4500 K (red giant, asymptotic giant branch stars (AGBs), and RSGs). We define a star as a RSG when it has a $T_{\rm eff}$ lower than 4500 K and a luminosity of $L/L_{\odot} > 10^4$, which corresponds to an initial mass of $\gtrsim 9\ M_{\odot}$ (Ekström et al. 2012). Late-type stars can easily be identified with *K* band spectroscopy, because of their strong CO band-head at 2.29 $\mu$m (e.g., Ivanov et al. 2004; Kleinmann & Hall 1986; Rayner et al. 2009; Wallace & Hinkle 1996). Near-infrared spectra of late-type stars (mostly Mira AGBs) may show continuum absorption by water. Water absorption affects both ends of the *H* band spectrum, from $\sim$ 1.4 $\mu$m to $\sim$ 1.55 $\mu$m, and from $\sim$ 1.75 $\mu$m to $\sim$ 1.80 $\mu$m, and the blue side of the *K* band from 2.0 $\mu$m to 2.1 $\mu$m (e.g., Alvarez et al. 2000; Blum et al. 2003; Comerón et al. 2004; Frogel & Whitford 1987; Rayner et al. 2009). Water absorption in *H* band is most easily detected, as a curved (pseudo)-continuum. Highly variable water absorption is found in Mira AGBs because of their pulsation (Matsuura et al. 2002). In Fig. 3, the stellar continua of stars 1 and 24 clearly show absorption by water.

For red giants and RSGs, the equivalent width of the CO band-head, EW(CO), can be used as a temperature indicator because it increases linearly with decreasing $T_{eff}$. Red giants and RSGs follow two different relations (Blum et al. 2003; Figer et al. 2006; Frogel & Whitford 1987); for a given temperature, RSGs have stronger CO bands than red giant stars. EW(CO)s of Miras are variables, do not correlate with $T_{eff}$ values, and their EW(CO)s may be as large as those of late RSGs

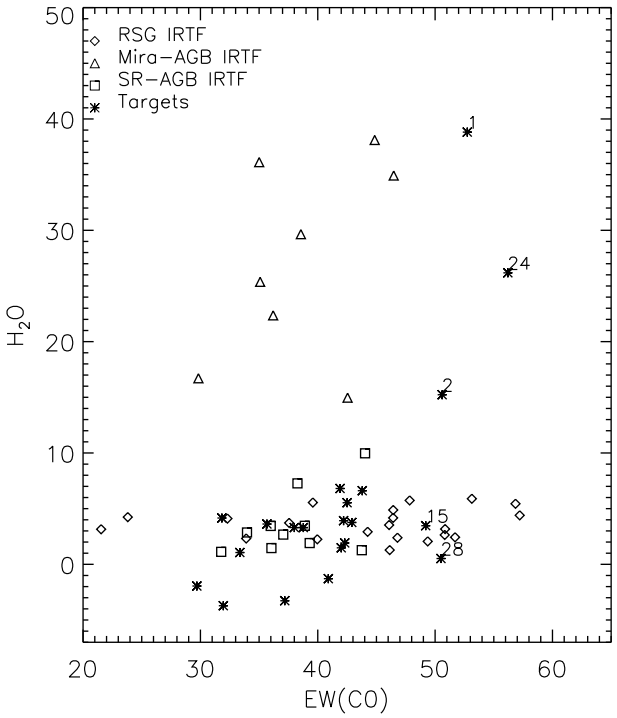


**Fig. 5.** $H_2O$ indexes versus the EW(CO)s of targeted late-type stars and comparison samples of AGBs (Mira and semi-regular variables) and RSGs from the IRTF library (Rayner et al. 2009).

(Blum et al. 2003). Water absorption decreases with increasing stellar luminosity (Blum et al. 2003; Frogel & Whitford 1987). All these considerations mean that combined information on water absorption and EW(CO) is useful for estimating luminosity classes.

We measured the EW(CO)s using the feature and continuum regions that are specified in Table 5; we obtained spectral types for the targets by comparing their EW(CO)s with those of reference spectra from the atlas of Kleinmann & Hall (1986); the reference spectra were smoothed to match the spectral resolution of the targets (e.g., Figer et al. 2006). Twelve targets were observed with both UIST and SOFI detectors; by comparing their resulting EW(CO)s, the typical accuracy of spectral types is found within two subclasses; star 24 is a Mira-like star that went from $> M7$ (UIST run) to M0 type (SOFI run). For spectra taken with the medium-resolution mode of SofI, we selected a narrower bandpass for the CO feature (see Table 5). A scaling factor of 1.4 was measured between the EW(CO)s from the medium-resolution SofI and those from UIST. For star 27, which was observed with both the low and medium modes of SofI, we obtained a RSG-type of K4 and K2, respectively. The degeneracy between RSGs and red giants disappears for EW(CO) values larger than $\sim 43 \pm 4$ Å. Miras stars, with their erratic behaviors, may also have EW(CO)s larger than 43 Å. Stars 1, 2, 15, 24, and 28 in Table 4 have EW(CO) values larger than 48; these stars are candidate AGBs or RSGs.

Water indexes were obtained from the de-reddened low-resolution SofI spectra, which cover *H* and *K* bands. We used a water index with continuum and absorption regions defined as in Blum et al. (2003). We measured the water index ($100 * (1 - < F_{\rm H_2O}/F_{continuum} >)$) with a quadratic fit to two continuum regions (see Table 5); $< F_{\rm H_2O}/F_{continuum} >$ is the average ratio of observed flux densities in the water region and estimated

**Table 4.** List of stars spectroscopically observed with UKIRT/UIST and NTT/SofI. Identification numbers are as in Table 3.

| | Photometry | | | Spectroscopy | | | | | | | | | | | |
|---|---|---|---|---|---|---|---|---|---|---|---|---|---|---|---|
| ID | *Q1* | *Q2* | var | EW(CO)[a] | | | sp_RSG[b] | | | sp_giant[c] | | | $H_2O$ | Comment | Instrument & mode[d] |
| | | | | UIST | SofII | SofIm | UIST | SofII | SofIm | UIST | SofII | SofIm | | | |
| | [mag] | [mag] | | [Å] | [Å] | [Å] | | | | | | | [%] | | |
| 1 | −0.24 ± 0.12 | ··· ± ··· | 0 | ··· | 53 | ··· | ··· | M1.5 | ··· | ··· | >M7 | ··· | 39 | sp_Mira_AGB | SofII |
| 2 | 0.04 ± 0.09 | −0.07 ± 0.09 | 0 | 51 | 52 | ··· | M1.5 | M1.5 | ··· | >M7 | >M7 | ··· | 15 | sp_Mira_AGB | SofII, UIST |
| 3 | 0.20 ± 0.09 | −0.26 ± 0.12 | 0 | 44 | ··· | ··· | K5.5 | ··· | ··· | >M7 | ··· | ··· | ··· | | UIST |
| 4 | 0.17 ± 0.13 | 0.62 ± 0.13 | 0 | 42 | 46 | ··· | K5 | M0 | ··· | M6.5 | >M7 | ··· | 7 | | SofII, UIST |
| 5 | 0.30 ± 0.21 | 1.13 ± 0.24 | 0 | ··· | 44 | ··· | ··· | K5.5 | ··· | ··· | >M7 | ··· | 7 | | SofII |
| 6 | 0.48 ± 0.13 | 1.03 ± 0.14 | 0 | ··· | 32 | ··· | ··· | K2 | ··· | ··· | M1.5 | ··· | 4 | | SofII |
| 7 | 0.21 ± 0.10 | 0.95 ± 0.15 | 0 | ··· | 36 | ··· | ··· | K3 | ··· | ··· | M3.5 | ··· | 4 | | SofII |
| 8 | ··· ± ··· | ··· ± ··· | 0 | ··· | 38 | ··· | ··· | K4 | ··· | ··· | M4.5 | ··· | 3 | | SofII |
| 9 | 0.30 ± 0.11 | 0.68 ± 0.15 | 0 | ··· | ··· | ··· | ··· | ··· | ··· | ··· | ··· | ··· | ··· | | SofII |
| 10 | 0.40 ± 0.11 | 0.40 ± 0.23 | 0 | ··· | 33 | ··· | ··· | K2.5 | ··· | ··· | M2.5 | ··· | 1 | | SofII |
| 11 | 0.11 ± 0.20 | −0.01 ± 0.51 | 0 | ··· | ··· | ··· | ··· | ··· | ··· | ··· | ··· | ··· | ··· | | SofII |
| 12 | 0.32 ± 0.14 | 0.26 ± 0.12 | 0 | 43 | 47 | ··· | K5 | M0 | ··· | M7 | >M7 | ··· | 6 | | SofII, UIST |
| 13 | −0.20 ± 0.18 | 0.07 ± 0.16 | 1 | ··· | ··· | ··· | ··· | ··· | ··· | ··· | ··· | ··· | ··· | | SofII, UIST |
| 14 | 0.24 ± 0.08 | 0.71 ± 0.11 | 1 | 42 | 45 | ··· | K5 | M0 | ··· | M7 | >M7 | ··· | 2 | | SofII, UIST |
| 15 | 0.23 ± 0.08 | 0.57 ± 0.11 | 0 | 49 | 45 | ··· | M1 | M0 | ··· | >M7 | >M7 | ··· | 3 | | SofII, UIST |
| 16 | 0.40 ± 0.09 | −0.22 ± 0.16 | 0 | 30 | 33 | ··· | K2 | K2.5 | ··· | M0.5 | M2 | ··· | −2 | | SofII, UIST |
| 17 | 0.08 ± 0.13 | ··· ± ··· | 1 | ··· | 37 | ··· | ··· | K3.5 | ··· | ··· | M4 | ··· | −3 | | SofII |
| 18 | 0.51 ± 0.09 | 0.90 ± 0.14 | 0 | ··· | 32 | ··· | ··· | K2.5 | ··· | ··· | M1.5 | ··· | −4 | | SofII |
| 19 | −0.04 ± 0.13 | 1.01 ± 0.66 | 1 | ··· | ··· | ··· | ··· | ··· | ··· | ··· | ··· | ··· | ··· | | SofII |
| 20 | −0.09 ± 0.16 | 0.13 ± 0.29 | 1 | ··· | ··· | ··· | ··· | ··· | ··· | ··· | ··· | ··· | ··· | | SofII |
| 21 | 0.44 ± 0.18 | 1.94 ± 0.97 | 1 | ··· | ··· | ··· | ··· | ··· | ··· | ··· | ··· | ··· | ··· | | SofII |
| 22 | 0.16 ± 0.08 | 0.96 ± 0.10 | 0 | 42 | 41 | ··· | K5 | K4.5 | ··· | M7 | M6 | ··· | 4 | | SofII, UIST |
| 23 | 0.22 ± 0.10 | −0.44 ± 0.11 | 0 | 44 | ··· | ··· | K5.5 | ··· | ··· | >M7 | ··· | ··· | ··· | | UIST |
| 24 | −0.15 ± 0.09 | −2.08 ± 0.12 | 1 | 56 | 29 | ··· | M3 | K1.5 | ··· | >M7 | M0 | ··· | 26 | sp_Mira_AGB | SofII, UIST |
| 25 | 0.28 ± 0.14 | 0.98 ± 0.11 | 0 | 41 | 39 | ··· | K5 | K4 | ··· | M6 | M5 | ··· | −1 | | SofII, UIST |
| 26 | −0.16 ± 0.21 | ··· ± ··· | 0 | ··· | ··· | ··· | ··· | ··· | ··· | ··· | ··· | ··· | ··· | | SofII |
| 27 | 0.25 ± 0.70 | −0.66 ± 1.42 | 0 | ··· | 39 | 31 | ··· | K4 | K2 | ··· | M5 | M0.5 | 3 | | SofII, SofIm |
| 28 | 0.39 ± 0.13 | 0.14 ± 0.10 | 0 | 51 | 50 | ··· | M1.5 | M1 | ··· | >M7 | >M7 | ··· | 1 | | SofII, UIST |
| 29 | 0.32 ± 0.12 | 0.53 ± 0.10 | 0 | 43 | 47 | ··· | K5.5 | M0 | ··· | M7 | >M7 | ··· | 4 | | SofII, UIST |
| 30 | 0.49 ± 0.11 | 0.84 ± 0.12 | 0 | 42 | 44 | ··· | K5 | K5.5 | ··· | M7 | >M7 | ··· | 1 | | SofII, UIST |
| 31 | 0.28 ± 0.14 | 0.67 ± 0.11 | 0 | ··· | ··· | 22 | ··· | ··· | <K0 | ··· | ··· | K3 | ··· | | SofIm |
| 32 | −0.24 ± 0.14 | −2.90 ± 0.11 | 0 | ··· | ··· | 28 | ··· | ··· | K1.5 | ··· | ··· | K5.5 | ··· | | SofIm |
| 33 | −0.15 ± 0.12 | −2.31 ± 0.09 | 0 | ··· | ··· | 27 | ··· | ··· | K1 | ··· | ··· | K5 | ··· | | SofIm |
| 34 | 0.28 ± 0.14 | 0.57 ± 0.13 | 1 | ··· | ··· | 21 | ··· | ··· | <K0 | ··· | ··· | K2 | ··· | | SofIm |
| 35 | 0.23 ± 0.13 | 0.44 ± 0.10 | 0 | ··· | ··· | 6 | ··· | ··· | <K0 | ··· | ··· | <K0 | ··· | | SofIm |
| 36 | 0.48 ± 0.10 | 0.80 ± 0.12 | 0 | ··· | ··· | 24 | ··· | ··· | <K0 | ··· | ··· | K3.5 | ··· | | SofIm |
| 37 | 0.46 ± 0.09 | 0.79 ± 0.12 | 0 | ··· | ··· | 24 | ··· | ··· | K0.5 | ··· | ··· | K3.5 | ··· | | SofIm |
| 38 | 0.36 ± 0.10 | 1.17 ± 0.12 | 0 | ··· | ··· | 30 | ··· | ··· | K2 | ··· | ··· | M0 | ··· | | SofIm |
| 39 | 0.03 ± 0.10 | 0.19 ± 0.20 | 0 | ··· | ··· | ··· | ··· | ··· | ··· | ··· | ··· | ··· | ··· | | SofIm |
| 40 | 0.30 ± 0.18 | ··· ± ··· | 0 | ··· | ··· | 22 | ··· | ··· | <K0 | ··· | ··· | K3 | ··· | | SofIm |
| 41 | 0.30 ± 2.78 | ··· ± ··· | 0 | ··· | ··· | 15 | ··· | ··· | <K0 | ··· | ··· | <K0 | ··· | | SofIm |
| 42 | 0.11 ± 0.12 | −0.22 ± 0.11 | 0 | 44 | ··· | ··· | K5.5 | ··· | ··· | >M7 | ··· | ··· | ··· | | UIST |
| 43 | 0.28 ± 0.09 | 0.89 ± 0.10 | 0 | 37 | ··· | ··· | K3.5 | ··· | ··· | M4 | ··· | ··· | ··· | | UIST |
| 44 | 0.32 ± 0.14 | 0.66 ± 0.12 | 0 | 28 | ··· | ··· | K1.5 | ··· | ··· | K5.5 | ··· | ··· | ··· | | UIST |
| 45 | 0.34 ± 0.09 | −0.32 ± 0.13 | 0 | 45 | ··· | ··· | M0 | ··· | ··· | >M7 | ··· | ··· | ··· | | UIST |
| 46 | 0.52 ± 0.09 | 0.90 ± 0.12 | 0 | 33 | ··· | ··· | K3 | ··· | ··· | M2.5 | ··· | ··· | ··· | | UIST |
| 47 | 0.51 ± 0.09 | 0.78 ± 0.12 | 0 | 24 | ··· | ··· | K0.5 | ··· | ··· | K4 | ··· | ··· | ··· | | UIST |
| 48 | 0.46 ± 0.09 | 0.85 ± 0.13 | 0 | 29 | ··· | ··· | K1.5 | ··· | ··· | M0 | ··· | ··· | ··· | | UIST |

**Notes:** ([a]) EW(CO)s from low-resolution SofI spectra were multiplied by a factor 1.4. ([b]) sp_RSG: spectral type by assuming a supergiant class. ([c]) sp_giant: spectral type by assuming a giant class. ([d]) SofII= low-resolution mode of SofI; SofIm= medium-resolution mode of SofI.

**Table 5.** Spectroscopic indexes. Spectral regions used as features and continuum are specified.

| Type | Band [$\mu$m] | Continuum [$\mu$m] | References | Comment |
|---|---|---|---|---|
| $H_2O$ | 2.0525-2.0825 | 1.68-1.72 | 1 | |
| | | 2.20-2.29 | 1 | |
| CO | 2.285-2.315 | 2.28-2.29 | | UIST, SofI Low |
| CO | 2.285-2.307 | 2.28-2.29 | | SofI medium |

**References:** (1) Blum et al. (2003).

flux densities (with a fit). For comparison, we estimated the EW(CO)s and water indexes of a sample of known AGBs and RSGs with spectra available from the IRTF library (Rayner et al. 2009). In Fig. 5, we plot water indexes versus EW(CO)s of the targets, as well as of reference spectra. A combination of water indexes and EW(CO)s allows us to distinguish between RSGs and Mira AGBs; we find that known Mira AGBs have water indexes greater than 15 Å, as in Blum et al. (2003). This confirms that targets 1, 2, and 24 are Mira-like stars. Water indexes for known RSGs and semi-regular AGBs (SR, e.g., Alard et al. 2001) are typically negligible; SR AGBs have EW(CO)s as large as $\sim$ 44 Å; RSGs up to $\sim$ 58 Å (see Fig. 5 and Table 4). SR AGBs contaminate the sample of spectroscopic candidate RSGs (EW(CO)$\gtrsim$ 43 Å); luminosities are crucial for classifying RSGs.

#### 4.1.2. Early-type stars

Low-resolution infrared spectra of O-, B-, A-, and F-type stars are characterized by hydrogen (H) lines (e.g., Hanson et al. 1996, 1998; Lancon & Rocca-Volmerange 1992; Rayner et al. 2009). The low-resolution SofI spectra of stars 9, 11, 13, 19, 20, 21, and 26 show H I lines in absorption at 1.555 $\mu$m, 1.570 $\mu$m, 1.588 $\mu$m, 1.611 $\mu$m, 1.641 $\mu$m, 1.681 $\mu$m, 1.737 $\mu$m, and 2.166 $\mu$m (see Fig. 3). The strengths of the hydrogen lines indicate types from B0 to F0 for stars 11, 13, 20, and 26; the presence of weak CO bands imply types from F5 to G5 for stars 9, 19, and 21.

A spectrum of star 39 was obtained with the medium-resolution mode SofI in $K$ band. A Br$\gamma$ in absorption and a He I at 2.1127 $\mu$m are detected. The presence of the He I line implies a B0-8 I, or a O9.5-B3V.

The coordinates and spectral types of early-type stars are listed in Tables 3 and 4.

#### 4.1.3. Photometric variability index

Mira AGBs are characterized by periodic photometric variations that can reach up to $\sim$ 1 mag in $K_s$ (Messineo et al. 2004). In contrast, only a small fraction of RSGs (about 20%) are known to vary, and typically RSGs have amplitudes of a few tenths of a magnitude in $K$ band (Yang & Jiang 2011).

Since the two DENIS and 2MASS $J$ filters are similar, we used both measurements for identifying candidate variable stars, i.e., stars with $J$(DENIS)> 7.5 mag, and $|J$(DENIS)$-J$(2MASS)$| > 3 \times 0.15$ mag, or with $K_s$ (DENIS)> 6.0 mag, and $|K_s$ (DENIS)$-K_s$ (2MASS)$| > 3 \times 0.15$ mag. For nonvariable stars, $|K_s$ (DENIS)$-K_s$ (2MASS)$|$ and $|J$(DENIS)$-J$(2MASS)$|$ are within 0.15 mag (Messineo et al. 2004; Schultheis et al. 2000). We also flagged as variables those targets with indication of variability from the shortest WISE band. The late-type stars 14, 17, 24, and 34 are candidate variables, as well as the early-types 13 and 20, and the $F$-$G$ stars 19 and 21. Star 24 is a Mira-like AGB, as inferred from the water index; the other variable late-type stars could be SR AGBs (Alard et al. 2001). None of the RSGs found has the variability flag on.

#### 4.1.4. Target intrinsic colors and interstellar extinction

For red giants and RSGs, we assumed the intrinsic $V-K$, $J-K$, and $H-K$ colors per spectral-type provided by Lejeune & Schaerer (2001) and Koornneef (1983). For each spectral type from K0 to M5, the $V-K$ (or $J-K$) colors of red giants and RSGs agree within 0.28 mag (or 0.09 mag), respectively (Koornneef 1983); this quantity is comparable to the color change between two neighboring subspectral types of the same luminosity class. We obtained intrinsic $I-J$ colors by interpolating a colored-isochrone of 6 Gyr and solar metallicity (Pietrinferni et al. 2004). The obtained $I-J$ colors of late-type giants agree with those of Lejeune & Schaerer (2001) for RSGs (4-30 Myr old) within 0.05 mag. The Koornneef photometric system agrees with the 2MASS system within 0.09 mag (Carpenter 2001).

For early-type stars, infrared-colors were taken from Bibby et al. (2008), Humphreys & McElroy (1984), Wegner (1994), Koornneef (1983), and Wainscoat et al. (1992).

For every target, we estimated $A_{K_s}$ with the assumed intrinsic colors, and a power-law extinction curve with an index of $-1.9$ (Messineo et al. 2005). This law yields an excellent agreement between estimates of $A_{K_s}$ from the observed ($I$-$J$), ($J-K_s$), and ($H-K_s$) colors. For eight stars with DENIS and 2MASS measurements, we obtained $A_{K_s}$(from $J-K_s$) $-$ $A_{K_s}$(from $I-J$) $=$ $-0.04$ mag with $\sigma$=0.14 mag; $A_{K_s}$(from $J-K_s$) $-$ $A_{K_s}$(from $H-K_s$) $=$ $-0.03$ mag with $\sigma$=0.09 mag.

Typically, we adopted the $A_{K_s}$ values from the ($J-K_s$) colors. For every field, an average extinction ($<A_{K_s}>$) was measured, as the average of the $A_{K_s}$ values of the observed late-type stars (with the exclusion of AGB stars). The field results are listed in Table 1. Stars with a value of $A_{K_s}$ that differs from the average extinction by more than three standard deviations were classified as foreground (background) sources, as indicated in Table 6. We used the shape of the continuum (quantified by the water index) to distinguish between objects with circumstellar envelopes (e.g., Mira AGB) and obscured, but naked, luminous objects.

### *4.2. Interstellar extinction as a distance indicator*

Distances were derived by matching the target $A_{K_s}$ value with a known curve of $A_{K_s}$ values versus distances (along the target line of sight). The targets are distributed in five fields along the Galactic plane, at galactic longitudes of 1.°5, 9.°5, 16.°7, 49.°3, and 59.°8, respectively, and approximately zero latitude.

A relation between $A_{K_s}$ and distance along a given line of sight can be derived with primary distance calibrators. Thanks to the availability of deep near-infrared surveys, such as VVV (Soto et al. 2013) and UKIDSS (Lucas et al. 2008), red clump stars (analogous to the Galactic horizontal branch stars in metal rich globular clusters) have been detected throughout the Galaxy, and may serve for this purpose (e.g., Drimmel et al. 2003; Gonzalez et al. 2011). We created UKIDSS $K$ versus $J-K$ diagrams of datapoints within $10' \times 10'$ from the cluster centers, and we visually selected by eyes the locus of a well visible red clump sequence. Per bin of $J-K$ color, we analyzed the distribution of

$K$ magnitudes (around the clump region), and estimated the peak of the red clump with a Gaussian fit. We assumed an intrinsic $(J-K)_o$ of 0.68 mag (Babusiaux & Gilmore 2005; Gonzalez et al. 2011) and an absolute magnitude in $K$ band, $M_{\rm K_s}$, of −1.61 mag (Alves 2000). Quoted values in the literature range from $M_{\rm K_s}$=−1.54, −1.55 mag (Groenewegen 2008; Pietrinferni et al. 2004) to $M_{\rm K_s}$=−1.72 mag (Babusiaux & Gilmore 2005). For all fields but one, distances were derived with clump stars in the $A_{\rm K_s}$ region of interest (average $A_{\rm K_s}$ of the targeted stars); for field cl59.8 it was not possible because there were not enough clump stars. For two fields, cl16.7 and cl49.3, it was possible to derived a curve of variation of $A_{\rm K_s}$ with distance (e.g., Drimmel et al. 2003), as shown in Fig. 6.

Alternatively, a curve of $A_{\rm K_s}$ versus distance along a given line of sight was derived with a model of Galactic dust distribution from COBE/DIRBE (Drimmel et al. 2003; Drimmel & Spergel 2001). A scaling factor of 0.74 was applied to transform the $A_{\rm K_s}$ of Drimmel et al. (2003) and Rieke & Lebofsky (1985) into the $A_{\rm K_s}$ derived with a power law of index=−1.9 (Messineo et al. 2005).

Estimated distances are listed in Table 1. In the following, we assume the distances derived with red clump stars. The Drimmel model tends to give shorter distances than those from the red clump fitting (Fig. 6); however, any detected RSGs would still be a RSG at the smaller distance provided by the Drimmel model.

In field cl49.3 it was possible to derive a spectrophotometric distance for star 39, an early B star with $K_{\rm s}$=11.19 mag. Typically, early-B stars have an absolute $K$ of $-6.45 \pm 0.42$ mag, $-3.52 \pm 1.00$ mag, or $-2.38 \pm 0.77$ mag, when they are supergiants (Ia), giants, or dwarfs, respectively (Bibby et al. 2008; Humphreys & McElroy 1984; Koornneef 1983; Wegner 1994). A supergiant class and a distance of 26 kpc can be excluded. By assuming a dwarf or a giant class, we derived a distance modulus (DM) of $13.02 \pm 0.77$ mag (4.0 kpc) and $14.16 \pm 1.00$ mag (6.8 kpc), respectively.

### 4.3. Estimated luminosities

Bolometric magnitudes, $M_{bol}$, and luminosities were calculated with $K_{\rm s}$ magnitudes, $A_{\rm K_s}$, estimated DMs, and bolometric corrections, $BC_{\rm K}$ (see Table 6). Values of $BC_{\rm K}$ per spectral type were taken from Levesque et al. (2005) and Messineo et al. (2011); the solar $M_{bol}$ was assumed to be +4.74 (Bessell et al. 1998).

For late-type stars, the spectral-energy distribution ($T_{\rm eff}$ from 4500 to 2000 K) peaks in the near-infrared (0.6-1.5 $\mu$m), or longward of this range when circumstellar dust is present (e.g., Figer et al. 2006; Ortiz et al. 2002). For late-types, we additionally integrated available flux densities over frequency $\nu$ using a linear interpolation. At short wavelengths, flux densities were extrapolated to zero with a blackbody function, at long wavelengths with a linear interpolation through the last two points. Direct integration yields more robust luminosities for dusty AGB stars, for which $BC_{\rm K}$ of naked stars are not applicable (Messineo 2004; Ortiz et al. 2002). The solar constant, $C_{\rm bol}$, was assumed to be −18.90. Our integration method provided $M_{bol}$ values in agreement within errors with those derived with the $BC_{\rm K}$ values.

Known RSGs have typical $M_{bol}$ from −5.5 mag to −9.0 mag (Clark et al. 2009; Davies et al. 2007; Figer et al. 2006). Galactic mass-losing AGB stars rarely exceed $M_{bol} \approx -7.1$ mag (Vassiliadis & Wood 1993); this theoretical limit may be exceeded with the onset of the hot bottom burning (HBB) process that breaks down the classic relation between core mass and luminosity (see, e.g., Groenewegen et al. 2009; Paczyński 1971). However, the efficiency of the HBB mechanism anti-correlates with metallicity, and it is usually associated with a stellar regime of high mass-loss and superwind (e.g., Marigo 2001; Vassiliadis & Wood 1993; Wood et al. 1983); typically, AGBs have strong water absorption in the bright end ($M_{bol}$ from −5.5 to −7 mag, Alard et al. 2001; Habing & Olofsson 2003). In the Milky Way, Mira AGBs have mostly late-types (M7-M9, as reported, for example, by Rayner et al. 2009); the distribution of spectral types of known RSGs peaks at M2-M4 (Davies et al. 2007).

For selecting clusters of RSGs, we calculated the photometric properties of the targets at the distance provided by their average $A_{\rm K_s}$ per field (as explained in Sect. 4.2); after having selected candidate RSGs, the procedure was reiterated with the $A_{\rm K_s}$ of the candidate RSGs. The results are summarized in Table 6. In field cl16.7 (DM=12.9 mag), stars 22 (K4.5-5I) and 23 (K5.5I) are two RSGs with $M_{bol}$=−6.18 mag and −5.71 mag. In field cl49.3 (DM=14.2 mag), star 27 (K4I) with a $M_{bol}$=−7.82 mag is a RSG star, along with the nearby stars 28 (M1-1.5I), 29 (K5.5-M0I), and 30 (K5-K5.5I), which have $M_{bol}$=−6.57 mag, −6.07 mag, and −5.76 mag, respectively. In none of these stars did we detect signs of variability or water absorption. There is only one Mira-like star exceeding $M_{bol}$=−5.5 mag in field cl1.5, which is star 1. For all other late-type stars, we estimated $M_{bol}$ typical of giant stars. There are a number of giants (after excluding the detected Mira-like AGBs) with estimated types later than M7III (3, 5, 12, 14, 15, 42, and 45); their $M_{bol}$ are below the values expected for faint RSGs.

## 5. Lines of sight towards cl16.7 and cl49.3

In the CMD of field cl16.7, at 16.°75 of longitude, and −0.°63 of latitude, the red clump trace is clearly visible from $J-K \approx 0.8$ mag and $K \approx 10$ mag to $J-K \approx 3.2$ mag and $K \approx 13.5$ mag (see Fig. 6). Clump stars appear evenly distributed along the line of sight, and their number increases with distance. For the RSGs in cl16.7, we derived an average $A_{\rm K_s}$ of 0.49 mag; from this $A_{\rm K_s}$, we obtained a DM of 12.93 mag, which places them on the Scutum-Crux arm (see Fig. 7, as well as the distribution of Galactic massive clusters in Messineo et al. 2009, 2014).

Field cl49.3 is located at a longitude of 49.°34 and a latitude of +0.°72. The DM inferred from the RSGs places the cluster cl49.3 onto the Sagittarius-Carina arm (see Fig. 7). In the CMD of field cl49.3, red clump stars are traceable from $J-K \approx 1$ mag and $K \approx 11.5$ mag to $J-K \approx 2.1$ mag and $K \approx 14.5$ mag (see Fig. 6). There is a sudden increase in the number of red clump stars at $J-K \approx 1.4$ mag, and a heliocentric distance larger than $\sim$ 5 kpc. This overdensity of red clump stars occurs at the shortest Galacto-centric distances along the line of sight, where the stellar density is higher; they are also encountered when tangentially approaching the Sagittarius-Carina arm (heliocentric distance 5-9 kpc, see Fig. 7). Similar structures appear in the CMDs of neighboring bins of longitudes. Some models predict the Galactic outer Linbland resonance to occur inside the solar circle, at a Galacto-centric distance of about 5 kpc (e.g., Habing et al. 2006); such resonances may generate/enforce extended structures (e.g., rings and pseudo-rings, Buta 1995). The Galactic long bar only extends to about $\lesssim 30^\circ$ longitude (Cabrera-Lavers et al. 2008).

## 6. Clusterings

Because of their young age most RSGs are mostly found in stellar clusters. Massive young clusters rich in RSGs have been identified via their near-infrared CMDs, e.g., the RSGC1 (Figer et al.

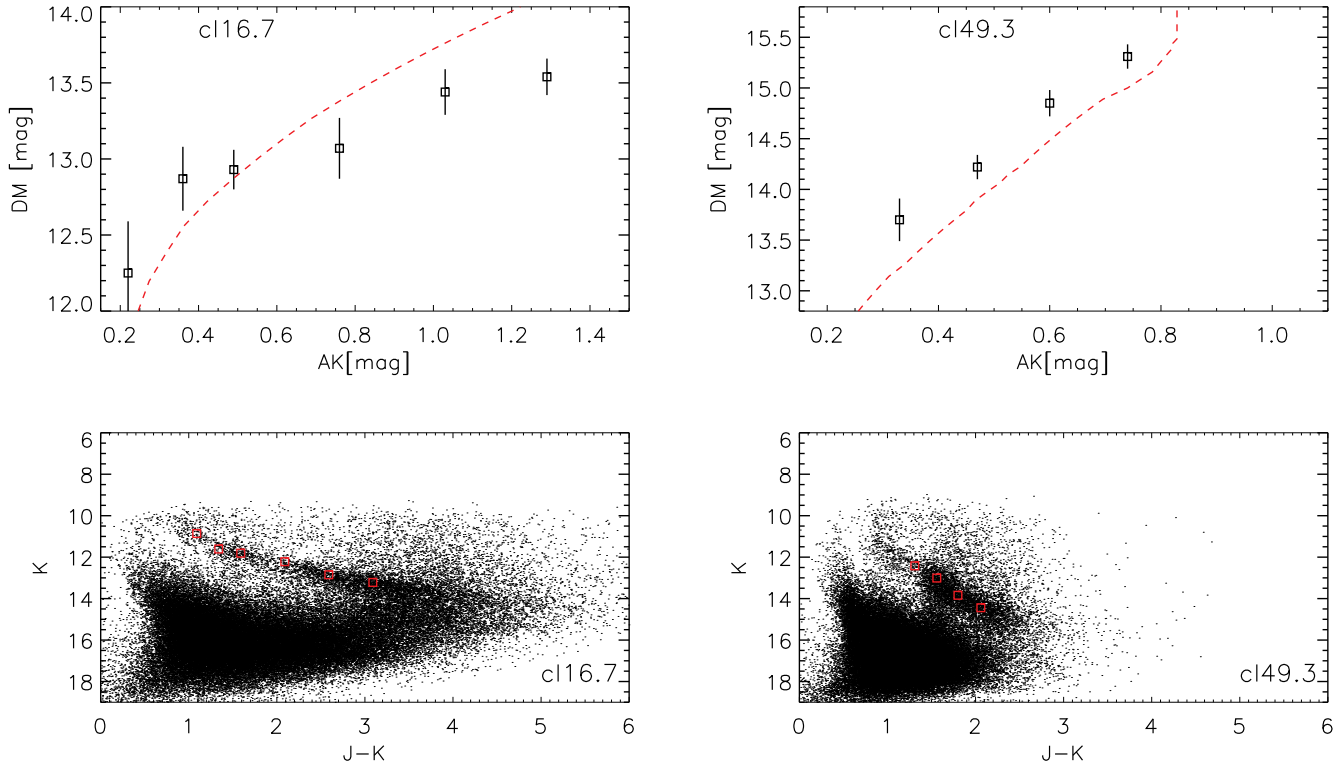


**Fig. 6.** *Top panels*: Interstellar extinction $A_K$ versus distance moduli of red clump stars in the fields of cl16.7 (*left*) and cl49.3 (*right*). As a comparison, the model of Drimmel et al. (2003) is shown with a dashed line. *Bottom panels*: UKIDSS $J-K$ versus $K$ diagram of data-points within an area of 10′×10′ from the estimated centers of cl16.7 (*left*) and cl49.3 (*right*).

2006), RSGC2 (Davies et al. 2007), and RSGC3 (Clark et al. 2009). In their ($J-K_s$) versus $K_s$ diagrams there are gaps of several magnitudes in $K_s$ between RSGs and blue supergiants (Figer et al. 2006); the gap inversely correlates with the cluster age (Figer et al. 2006; Messineo et al. 2009). For comparison, Mira AGBs are typically isolated on a scale of 1′ and are among the brightest stars, but are typically the reddest (Messineo et al. 2004, 2005); in the CMDs of stars surrounding Mira stars gaps may only be present stochastically.

The CMDs of the analyzed candidate clusters are shown in Fig. 8. The CMDs of fields cl16.7 and cl49.3 are characterized by gaps; in these two fields we detected several stars with luminosities typical of RSGs. The infrared CMDs nicely complement and strengthen the detection of six new RSGs, as illustrated in the following.

### 6.1. RSGs in field cl16.7

The 2MASS/UKIDSS ($J-K_s$) versus $K_s$ diagram of field cl16.7 shows two bright RSGs (stars 22 and 23) at ($J-K_s$)≈ 1.9 mag and $K_s$≈ 4.8 mag (Fig. 8). The two RSGs (stars 22 and 23) have similar extinction values ($A_{K_s}$=0.46 and 0.52 mag), and spectral types, and so they are drawn from the same population. The CMD shows a group of bright stars that extends over a main sequence to about 9.5 mag. There is a gap of about 4.5 mag between these stars and the two RSGs. The two other bright stars with $K_s$=5.91 and 6.64 mag are field giant stars.

Star 26 (early or yellow-type) has $A_{K_s}\sim$ 0.58 mag, which is consistent with the extinction of the two RSGs. On the CMD, the star is located at (J-$K_s$)=1.0 mag and $K_s$=12.1 mag, over a main sequence (from $K_s$=18 mag to 14 mag). It is probably not related to the young RSGs; for DM=12.9 mag, we obtain $M_{K_s}$=−1.4 mag (typical of old late-B giants, see, e.g., Clampitt & Burstein 1997).

Star 24 is 5″ from the IRAS 18207−1441 source, within its positional error ellipse. Its spectrum has strong water absorption. A few rare RSGs have shown water absorption in $H$ band, e.g., My Cep (M7I) in NGC 7419 (Rayner et al. 2009). My Cep, the brightest of the five RSGs in NGC7419, is a pulsating star, and shows OH and water masers (Benson et al. 1990). Star 24 can be a late giant (M8III) or a faint M3I with an integrated Mbol of −4.97 mag. Since the two RSGs (K5I, K5.5I) are bluer and brighter (Mbol=−6.2 and −5.7 mag) than star 24, we concluded that this was most likely an unrelated AGB star. Accurate radial velocities are needed to confirm the proposed scenario.

A colored theoretical isochrone from Lejeune & Schaerer (2001), with increased mass loss, solar metallicity, and an age of 20 Myr, is overplotted on the CMD of field cl16.7 in Fig. 8. The isochrone is shifted to the assumed cluster distance, and reddened. It encompasses the RSGs, as well as the early-type giant star 26.

For the two RSGs, we derived luminosities of $2.3\times10^4$ and $1.5\times10^4$ $L_\odot$ (see Table 6). In Fig. 10, luminosities are plotted versus effective temperatures, and compared to theoretical stellar tracks by Ekström et al. (2012); we used tracks at solar metallic-

**Table 6.** Photometric properties of the targeted stars.

| ID | rad | Fields | $K_S$ | Sp* | $(J-K_S)_o$ | $A_{K_s}(JK_s)$ | $A_{K_s}(HK_s)$ | $A_{K_s}(IJ)$ | $M_K$ | DM | $BC_K$ | $M_{bol1}$ | $M_{bol2}$ | Notes** |
|---|---|---|---|---|---|---|---|---|---|---|---|---|---|---|
| | [′] | | [mag] | | [mag] | [mag] | [mag] | [mag] | [mag] | [mag] | [mag] | [mag] | [mag] | |
| 1 | 3.30 | cl1.5 | 4.86 | M8IIIM | 1.42 | 0.64 | 0.89 | ··· | -10.32 ± 0.17 | 14.54 ± 0.16 | 3.34 ± 0.11 | -6.98 ± 0.21 | -7.55 ± 0.33 | |
| 2 | 0.09 | cl1.5 | 7.35 | M8IIIM | 1.42 | 0.49 | 0.58 | ··· | -7.68 ± 0.17 | 14.54 ± 0.16 | 3.34 ± 0.11 | -4.33 ± 0.21 | -4.59 ± 0.32 | |
| 3 | 0.37 | cl1.5 | 8.09 | M8III | 1.42 | 0.57 | 0.58 | ··· | -7.02 ± 0.18 | 14.54 ± 0.16 | 3.34 ± 0.11 | -3.67 ± 0.21 | -3.92 ± 0.33 | |
| 4 | 0.24 | cl1.5 | 8.54 | M6.5III | 1.33 | 0.38 | 0.44 | ··· | -6.38 ± 0.18 | 14.54 ± 0.16 | 3.15 ± 0.11 | -3.23 ± 0.21 | -3.39 ± 0.36 | |
| 5 | 1.81 | cl1.5 | 8.81 | M8III | 1.42 | 0.32 | 0.28 | ··· | -6.05 ± 0.19 | 14.54 ± 0.16 | 3.34 ± 0.11 | -2.71 ± 0.22 | -3.00 ± 0.40 | |
| 6 | 0.10 | cl1.5 | 9.01 | M1.5III | 1.02 | 0.55 | 0.51 | ··· | -6.08 ± 0.17 | 14.54 ± 0.16 | 2.76 ± 0.10 | -3.32 ± 0.20 | -3.42 ± 0.32 | |
| 7 | 2.92 | cl1.5 | 9.07 | M3.5III | 1.13 | 0.40 | 0.51 | ··· | -5.87 ± 0.18 | 14.54 ± 0.16 | 2.88 ± 0.11 | -2.99 ± 0.21 | -3.08 ± 0.36 | |
| 8 | 4.15 | cl1.5 | 10.06 | M4.5III | 1.20 | ··· | 0.53 | ··· | ··· | 14.54 ± 0.16 | 2.89 ± 0.11 | ··· | -2.43 ± 0.21 | |
| 9 | 2.04 | cl1.5 | 10.08 | F5G5 | 0.34 | 0.31 | 0.22 | ··· | -4.77 ± 0.16 | 14.54 ± 0.16 | ··· | ··· | ··· | |
| 10 | 3.68 | cl1.5 | 10.23 | M2.5III | 1.07 | 0.46 | 0.45 | ··· | -4.76 ± 0.17 | 14.54 ± 0.16 | 2.83 ± 0.09 | -1.93 ± 0.20 | -2.06 ± 0.35 | |
| 11 | 0.43 | cl1.5 | 12.24 | B0F0 | −0.06 | 0.16 | 0.09 | ··· | 0.89 ± 0.80 | 11.19 ± 0.80 | ··· | ··· | ··· | FG |
| 12 | 0.24 | cl9.5 | 6.39 | M7III | 1.36 | 0.63 | 0.60 | 0.55 | -8.29 ± 0.14 | 14.05 ± 0.12 | 3.21 ± 0.11 | -5.08 ± 0.18 | -5.25 ± 0.32 | |
| 13 | 0.21 | cl9.5 | 7.83 | B0F0/A0III | 0.09 | 0.04 | 0.17 | ··· | −1.10 ± 0.80 | 8.90 ± 0.80 | ··· | ··· | ··· | FG |
| 14 | 0.27 | cl9.5 | 8.02 | M7III | 1.36 | 0.73 | 0.74 | 0.83 | -6.76 ± 0.14 | 14.05 ± 0.12 | 3.21 ± 0.11 | -3.55 ± 0.18 | -3.69 ± 0.31 | |
| 15 | 0.16 | cl9.5 | 8.13 | M8III | 1.42 | 0.73 | 0.72 | ··· | -6.65 ± 0.14 | 14.05 ± 0.12 | 3.34 ± 0.11 | -3.30 ± 0.18 | -3.55 ± 0.29 | |
| 16 | 0.29 | cl9.5 | 8.84 | M0.5III | 0.99 | 0.87 | 0.87 | 0.84 | -6.08 ± 0.13 | 14.05 ± 0.12 | 2.71 ± 0.10 | -3.36 ± 0.17 | -3.45 ± 0.26 | |
| 17 | 1.05 | cl9.5 | 9.49 | M4III | 1.16 | 0.70 | 0.88 | 0.64 | -5.27 ± 0.14 | 14.05 ± 0.12 | 2.89 ± 0.11 | -2.38 ± 0.18 | ··· ± ··· | |
| 18 | 1.30 | cl9.5 | 9.60 | M1.5III | 1.02 | 0.59 | 0.54 | 0.67 | -5.04 ± 0.13 | 14.05 ± 0.12 | 2.76 ± 0.10 | -2.28 ± 0.17 | -2.37 ± 0.30 | |
| 19 | 1.81 | cl9.5 | 11.76 | F5G5 | 0.34 | 0.01 | 0.07 | ··· | 5.82 ± 0.80 | 5.93 ± 0.80 | ··· | ··· | ··· | FG |
| 20 | 2.37 | cl9.5 | 11.77 | B0F0 | −0.06 | 0.36 | 0.40 | ··· | -2.65 ± 0.13 | 14.05 ± 0.12 | ··· | ··· | ··· | |
| 21 | 0.92 | cl9.5 | 12.49 | F5G5 | 0.34 | 0.75 | 0.58 | ··· | -2.30 ± 0.13 | 14.05 ± 0.12 | ··· | ··· | ··· | |
| 22 | 0.52 | cl16.7 | 4.55 | K5I | 0.96 | 0.46 | 0.59 | 0.54 | -8.84 ± 0.15 | 12.93 ± 0.13 | 2.66 ± 0.10 | -6.18 ± 0.18 | -6.24 ± 0.36 | |
| 23 | 0.38 | cl16.7 | 5.06 | K5.5I | 0.98 | 0.52 | 0.62 | 0.87 | -8.39 ± 0.15 | 12.93 ± 0.13 | 2.68 ± 0.10 | -5.71 ± 0.18 | -5.79 ± 0.35 | |
| 24 | 0.71 | cl16.7 | 5.92 | M8IIIM | 1.42 | 1.29 | 1.49 | 0.24 | -8.31 ± 0.15 | 12.93 ± 0.13 | 3.34 ± 0.11 | -4.97 ± 0.18 | -5.37 ± 0.30 | |
| 25 | 0.61 | cl16.7 | 6.64 | M6III | 1.30 | 0.63 | 0.65 | 0.52 | -6.91 ± 0.15 | 12.93 ± 0.13 | 3.08 ± 0.11 | -3.83 ± 0.18 | -3.98 ± 0.31 | |
| 26 | 1.10 | cl16.7 | 12.10 | B0F0 | −0.06 | 0.58 | 0.66 | ··· | -1.41 ± 0.15 | 12.93 ± 0.13 | ··· | ··· | ··· | |
| 27 | 0.59 | cl49.3 | 4.12 | K4I | 0.79 | 0.31 | 0.34 | ··· | -10.41 ± 0.46 | 14.22 ± 0.12 | 2.59 ± 0.10 | -7.82 ± 0.47 | -7.99 ± 0.74 | |
| 28 | 0.92 | cl49.3 | 5.41 | M1.5I | 1.03 | 0.51 | 0.51 | ··· | -9.32 ± 0.14 | 14.22 ± 0.12 | 2.76 ± 0.10 | -6.57 ± 0.17 | -6.66 ± 0.31 | |
| 29 | 1.45 | cl49.3 | 5.97 | K5.5I | 0.98 | 0.50 | 0.54 | ··· | -8.75 ± 0.14 | 14.22 ± 0.12 | 2.68 ± 0.10 | -6.07 ± 0.17 | -6.15 ± 0.34 | |
| 30 | 0.72 | cl49.3 | 6.38 | K5I | 0.96 | 0.57 | 0.53 | ··· | -8.42 ± 0.15 | 14.22 ± 0.12 | 2.66 ± 0.10 | -5.76 ± 0.18 | -5.84 ± 0.35 | |
| 31 | 3.59 | cl49.3 | 7.16 | K3III | 0.80 | 0.21 | 0.25 | ··· | -7.27 ± 0.14 | 14.22 ± 0.12 | 2.53 ± 0.10 | -4.74 ± 0.17 | -4.86 ± 0.35 | |
| 32 | 3.86 | cl49.3 | 7.40 | K5.5III | 0.97 | 0.97 | 1.31 | ··· | -7.79 ± ··· | 14.22 ± 0.12 | 2.68 ± 0.10 | -5.11 ± ··· | -5.25 ± 0.28 | |
| 33 | 5.10 | cl49.3 | 7.92 | K5III | 0.96 | 1.18 | 1.47 | ··· | -7.48 ± ··· | 14.22 ± 0.12 | 2.66 ± 0.10 | -4.82 ± ··· | -4.95 ± 0.31 | |
| 34 | 3.05 | cl49.3 | 8.06 | K2III | 0.68 | 0.21 | 0.22 | ··· | -6.38 ± 0.14 | 14.22 ± 0.12 | 2.46 ± 0.03 | -3.91 ± 0.14 | -4.08 ± 0.33 | |
| 35 | 5.02 | cl49.3 | 8.09 | K0III | 0.64 | 0.07 | 0.10 | ··· | -6.20 ± 0.14 | 14.22 ± 0.12 | 2.54 ± 0.03 | -3.66 ± 0.14 | -3.90 ± 0.32 | |
| 36 | 1.43 | cl49.3 | 8.39 | K3.5III | 0.84 | 0.52 | 0.46 | ··· | -6.35 ± 0.14 | 14.22 ± 0.12 | 2.56 ± 0.10 | -3.79 ± 0.17 | -3.90 ± 0.31 | |
| 37 | 1.12 | cl49.3 | 10.07 | K3.5III | 0.84 | 0.59 | 0.54 | ··· | -4.74 ± 0.14 | 14.22 ± 0.12 | 2.56 ± 0.10 | -2.18 ± 0.17 | -2.29 ± 0.32 | |
| 38 | 1.31 | cl49.3 | 10.24 | M0III | 0.97 | 0.83 | 0.84 | ··· | -4.81 ± 0.13 | 14.22 ± 0.12 | 2.70 ± 0.10 | -2.11 ± 0.16 | -2.19 ± 0.27 | |
| 39 | 0.86 | cl49.3 | 11.19 | O9.5-B3 | −0.13 | 0.56 | 0.51 | ··· | −3.58 ± 0.12 | 14.22 ± 0.12 | −2.53 ± 0.87 | −6.11 ± 0.88 | ··· | |
| 40 | 5.80 | cl49.3 | 11.29 | K3III | 0.80 | 0.78 | 0.81 | ··· | -3.71 ± 0.15 | 14.22 ± 0.12 | 2.53 ± 0.10 | -1.19 ± 0.18 | ··· ± ··· | |
| 41 | 1.36 | cl49.3 | 11.48 | K0III | 0.64 | 0.24 | 0.23 | ··· | -2.98 ± 0.64 | 14.22 ± 0.12 | 2.54 ± 0.03 | -0.44 ± 0.64 | ··· ± ··· | |
| 42 | 0.34 | cl59.8 | 6.49 | M8III | 1.42 | 0.56 | 0.61 | ··· | -6.92 ± 1.39 | 12.85 ± 1.39 | 3.34 ± 0.11 | -3.58 ± 1.40 | -3.82 ± 1.56 | |
| 43 | 0.26 | cl59.8 | 6.73 | M4III | 1.16 | 0.37 | 0.43 | ··· | -6.49 ± 1.39 | 12.85 ± 1.39 | 2.89 ± 0.11 | -3.60 ± 1.40 | -3.69 ± 1.56 | |
| 44 | 0.28 | cl59.8 | 6.97 | K5.5III | 0.97 | 0.06 | 0.09 | ··· | -5.93 ± 1.39 | 12.85 ± 1.39 | 2.68 ± 0.10 | -3.25 ± 1.40 | -3.35 ± 1.54 | |
| 45 | 0.72 | cl59.8 | 8.22 | M8III | 1.42 | 0.79 | 0.72 | ··· | -5.42 ± ··· | 12.85 ± 1.39 | 3.34 ± 0.11 | -2.07 ± ··· | -2.36 ± 1.56 | |
| 46 | 0.47 | cl59.8 | 8.39 | M2.5III | 1.07 | 0.42 | 0.36 | ··· | -4.88 ± 1.39 | 12.85 ± 1.39 | 2.83 ± 0.09 | -2.05 ± 1.40 | -2.17 ± 1.56 | |
| 47 | 0.84 | cl59.8 | 8.54 | K4III | 0.88 | 0.11 | 0.04 | ··· | -4.42 ± 1.39 | 12.85 ± 1.39 | 2.59 ± 0.10 | -1.83 ± 1.40 | -1.94 ± 1.59 | |
| 48 | 0.95 | cl59.8 | 9.03 | M0III | 0.97 | 0.36 | 0.32 | ··· | -4.17 ± 1.39 | 12.85 ± 1.39 | 2.70 ± 0.10 | -1.48 ± 1.40 | -1.59 ± 1.53 | |

**Notes:** Identification numbers are followed by distances to the centers of the stellar overdensities, field names, $K_s$, spectral types, $(J-K_s)_o$, $A_{K_s}(J-K_s)$, $A_{K_s}(H-K_s)$, $A_{K_s}(I-J)$, absolute $K_s$ ($M_{K_s}$), distance modulus (DM), bolometric corrections ($BC_K$), and bolometric magnitudes. $M_{bol1}$ are obtained via $BC_K$, and $M_{bol2}$ via direct integration. (*) The M suffix indicates a Mira-like star. (**) The FG comment indicates that this star has an $A_{K_s}$ at least three times smaller than the average of the targets in the field. Its distance was estimated with Drimmel model (a significant number of clump stars were not available at this $A_{K_s}$). The quoted DM error (0.8 mag) was estimated from Fig. 6.

ity that include rotation; the RSGs had initial masses from 10 $M_\odot$ to 13 $M_\odot$.

### 6.2. RSGs in field cl49.3

In field cl49.3, we detected four RSGs (27, 28, 29, and 30). The four RSGs have similar $A_{K_s}$($A_{K_s}$=0.47 ± 0.11 mag), and spectral types (from K4 to M1.5); their $K_s$ range from 4.1 mag to 6.4 mag. The $J-K_s$ versus $K_s$ diagram presents a gap of about 2 mag between the RSGs and other fainter stars (Fig. 8).

The O9.5-B3 star 39 is 4.8 mag fainter than the group of RSGs, and has $A_{K_s}$=0.56 mag. The spectro-photometric properties of star 39 indicate a giant (DM=14.16 mag) or a dwarf (DM=13.02 mag). The similarity of reddening suggests that the giant 39 and the four RSGs are at the same distance, and could belong to the same coeval population; an isochrone of 20 Myr (Lejeune & Schaerer 2001) encompass both the RSGs and the colors and magnitudes of star 39.

The bulk of stars at $K$ =11-12.5 mag and $J-K \approx 1$ mag is made of red clump stars (see Sect. 5 and Fig. 6). Among them we found six blue stars and star 39 (see Fig. 9). These blue stars appear radially concentrated towards the RSGs, and may be unrelated to the population of clump stars; late-types and early-types have different intrinsic colors ($J-K = 0.7-0.8$ mag for late, and ≈ 0.0 mag for early-type stars), and the red clump of stars at $J-K \approx 1$ mag is in the foreground of star 39.

For the assumed distance (DM=14.2 ± 0.1 mag from clump stars), the luminosities of RSGs range from $1.6 \times 10^4$ $L_\odot$ to $1.1{\times}10^5$ $L_\odot$. From a comparison with the tracks by Ekström et al. (2012), we estimate initial masses from 12 $M_\odot$ to 15 $M_\odot$ (see Fig. 10).

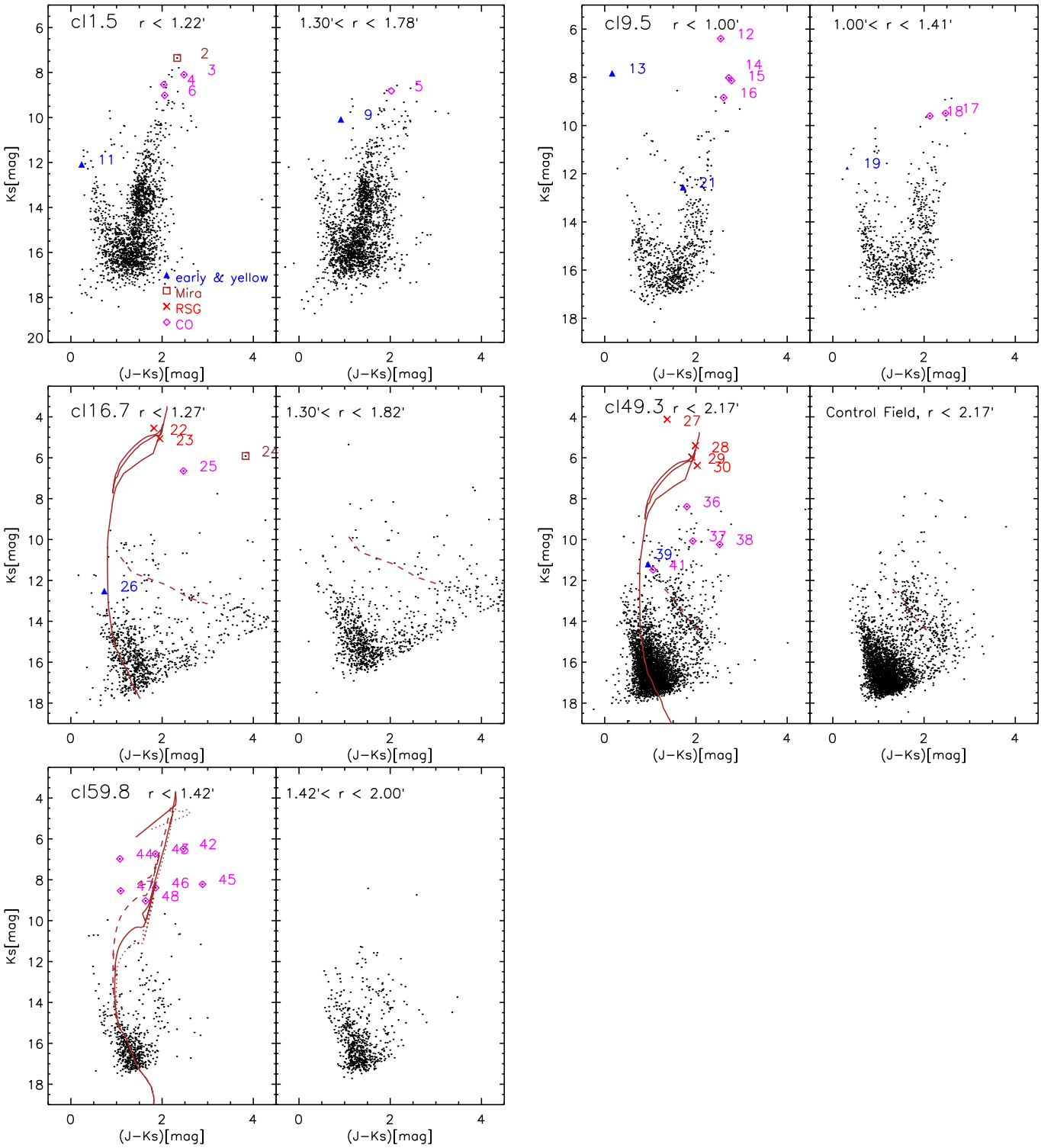


**Fig. 8.** 2MASS/UKIDSS $J - K_S$ versus $K_S$ CMDs: cl1.5 (*top left*), cl9.5 (*top right*), cl16.3 (*middle left*), cl49.3 (*middle right*), and cl59.8 (*bottom left*). Photometry was obtained with a PSF-fitting technique (see text). For each candidate cluster, a diagram of the candidate cluster is shown in the left panel, and that of a control field of equal area in the right panel. Spectroscopically detected early and yellow stars are marked with filled triangles, Miras with squares, RSGs with crosses, and red giants with diamonds; identification numbers are taken from Table 3. In the CMDs of fields cl16.3 and cl49.3, which are rich in RSGs, a continuous curve displays an isochrone of 20 Myr from Lejeune & Schaerer (2001), reddened with $A_{K_s}$=0.50 mag and 0.48 mag, and shifted to DM= 12.93 mag and 14.22 mag, respectively; a dashed line shows the sequence of red clump stars (see Sect. 4.2). The CMD of cl59.8 shows three isochrones from Marigo et al. (2008) with solar metallicity and ages of 100 (dashed line), 200 (continuous line), and 300 Myr (dotted line), which were reddened ($A_{K_s}$=0.55 mag) and shifted to DM=12.9 mag.

### *6.3. Other fields*

Field cl59.8 contains seven bright stars with $K_s$ from 6.5 mag to 9 mag. For the estimated DM= 12.9 ± 1.4 mag, these stars have

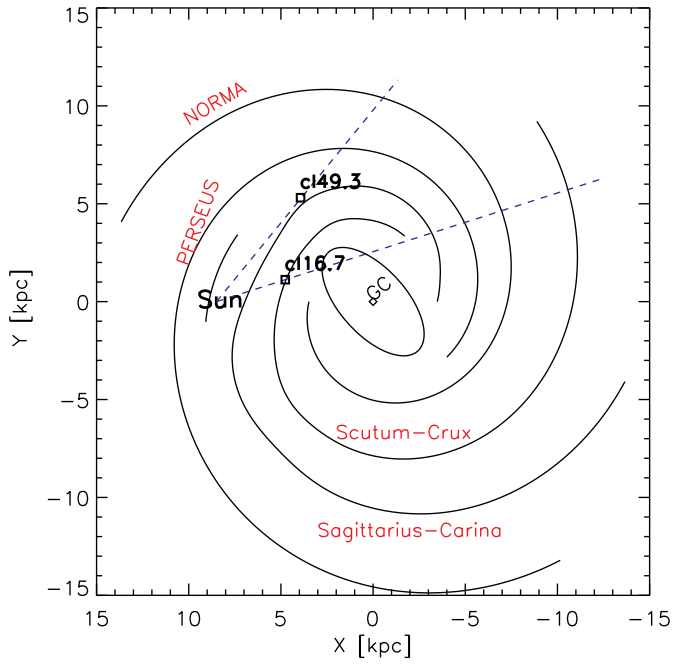


**Fig. 7.** XY view of the Milky Way. The Galactic center is at (0,0) and the Sun is at (8,0). The dashed lines indicate the line of sights to cl16.7 and cl49.3, which are marked with squares. A sketch of the spiral structure is also drawn and the arms are labeled (Cordes & Lazio 2002). The X-axis is oriented along the Sun-Galactic center line of sight.

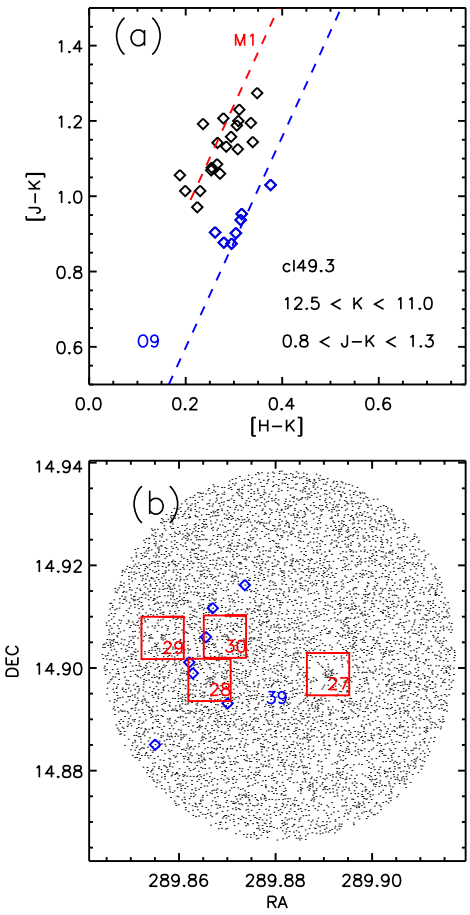


**Fig. 9.** Panel (a) shows a $(J-K)$ versus $(H-K)$ diagram of stars with $12.5 < K < 11$ mag and $0.8 < J-K < 1.3$ mag in the cl49.3 field. The dashed lines show the locus of a M1 and an O9 star for increasing $A_{K_s}$. Panel (b) shows a map of the blue stars (diamonds), along with the detected RSGs (squares) and field stars (dots).

typical bolometric magnitudes of giant stars. Nevertheless, they form a statistically significant overdensity of bright stars. The CMD of field cl59.8 is shown in Fig. 8. Stars 44 and 47 are bluer ($A_{K_s}$=0.06 and 0.11 mag), and are likely in the foreground. Star 45 has $A_{K_s}$=0.79 mag, and is a possible background object. For the remaining four stars, 42, 43, 46, and 48, $A_{K_s}$ range from 0.36 mag to 0.56 mag, and luminosities increase with spectral types; they are consistent with massive giants drawn from a population older than 100 Myr (Marigo et al. 2008). The infrared CMDs of simple stellar populations from 50 Myr to 200 Myr show gaps and a large number of bright giants, e.g., the GLIMPSE13 cluster (Messineo et al. 2009).

The CMDs of fields cl1.5 and cl9.5 do not present peculiar gaps or overdensities of stars brighter than $K_s$=7 mag (see Table 2). In conclusion, fields cl1.5 and cl9.5 are populated by older stars (> 600 Myr; Ferraro et al. 1995).

Field cl1.5 appears as a window of low extinction at the distance of the Galactic center with an inferred DM=14.54 ± 0.16 mag, and an average $A_{K_s}$=0.45 ± 0.08 mag; this result is in agreement with the extinction map by Gonzalez et al. ( 2012). Spectroscopically detected giant stars within < 2′ from the center of cl1.5 have $K_s$ from 7.52 mag to 8.55 mag; since the tip of the red giant branch (RGB) is expected at $K \approx 8.2$ mag (Glass et al. 1995; Messineo et al. 2005), they are most likely AGBs. The Mira-like star 2 is above the RGB tip ($K_s$=6.86 mag). The Mira-like AGB 1 is 3.′3 from the center, and has $K_s$=4.86 mag and $M_{bol}$= −6.98 mag for the assumed DM, which is compatible with the maximum luminosities predicted for Mira stars (see Fig. 20 in Vassiliadis & Wood 1993).

### 6.4. The Q1 and Q2 parameters

Messineo et al. (2012) analyzed Galactic stars of known types with the following parameters:

$$Q1 = (J-H) - 1.8 \times (H-K_s),$$

$$Q2 = (J-K_s) - 2.69 \times (K_s - [8.0]).$$

These two parameters are interstellar extinction free, and measure the distance of a datapoint from the Galactic reddening vector (passing trough the origin) in the $J-H$ versus $H-K_s$ ($Q1$), and $J-K_s$ versus $K_s-[8.0]$ planes ($Q2$). Typically, early-type stars have $Q1 < -0.20 \times (K_S - [8.0]) + 0.34$ mag (Messineo et al. 2012). A fraction of 72% of the spectroscopic targets are correctly classified into late- and early-type stars by applying the above relation. The $Q1$ and $Q2$ parameters only allow the selection of stars with colors typical of RSGs. Additional information on distances and luminosities is needed to classify RSGs. Messineo et al. (2012) calculated that 72% of known RSGs fall into the region 0.1 mag < $Q1$ < +0.5 mag and −1.1 mag < $Q2$ < +1.5 mag; five of the six new RSGs fall in this region, their average $Q1$=0.3 mag with $\sigma$=0.12 mag; in contrast,

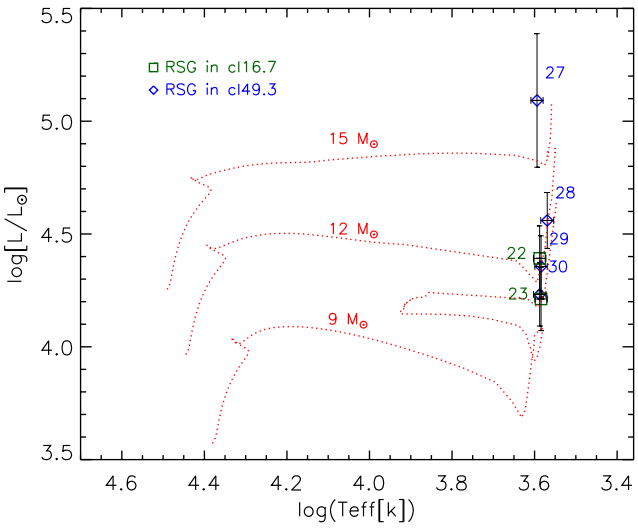


**Fig. 10.** Luminosities versus effective temperatures of the newly detected RSGs. RSGs in field cl16.7 are marked with squares, RSGs in field cl49.3 with diamonds. Stellar tracks for stars of 9, 12, and 15 $M_{\odot}$, from the new rotating Geneva models with a solar metallicity (Ekström et al. 2012), are shown with dotted lines.

detected Mira-like stars have an average $Q1 = -0.11$ mag with $\sigma$=0.14 mag.

## 7. Summary and discussion

The detection of clusters rich in RSGs is strongly affected by biases. It is difficult to classify and detect RSGs, because of our poor knowledge on distance, and because of the high and patchy extinction in direction of the Galactic plane. Nevertheless, their census is of importance to understanding the history of Galactic chemical enrichment, modality of star formation, and Galactic structure.

We conducted infrared spectroscopic observations of five overdensities with bright stars, which were detected with GLIMPSE and 2MASS data along the Galactic plane. We obtained 48 stellar spectra, and assigned spectral types to 47 new stars.

Late-type stars were classified using photometric data and spectroscopic indexes (water indexes and EW(CO)s). High values of the water index showed that stars 1, 2, and 24 were Mira-like AGBs. We detected six new RSGs (22, 23, 27, 28, 29, and 30) via their large EW(CO)s, low water indexes, and luminosities ( $> 10^4\ L_{\odot}$). All but one of the RSGs have EW(CO) > 42Å.

Clustering of candidate RSGs and gaps in the CMDs are powerful tools for detecting RSGs. The detected RSGs are in two fields, cl16.7 and cl49.3. Each group of RSGs presents narrow ranges of $A_{K_s}$ and $K_s$ magnitudes. Stars 22 and 23 fall in field cl16.7, and stars 27, 28, 29, and 30 in field cl49.3. The CMDs of both fields show large gaps between the RSGs and the group of blue giant/supergiants extending over a main sequence; this gap is a typical feature of clusters rich in RSGs (e.g., Figer et al. 2006).

The two RSGs in field cl16.7 are located at a heliocentric distance of ~ 3.9 kpc, at a Galactic longitude of 16.7° on the the Scutum-Crux arm. The two RSGs had stellar initial masses from 11 $M_{\odot}$ to 13 $M_{\odot}$.

The cluster of four RSGs in field cl49.3 is at a distance of ~ 7.0 kpc, at 49.°3 of galactic longitude on the Sagittarius-Carina arm. The RSGs had initial masses of 12 $M_{\odot}$ to 15 $M_{\odot}$.

By using multiwavelength analysis, and a measure of dust obscuration with distance, it is possible to isolate far distant and luminous objects, and groups of candidate RSGs. However, spectroscopic confirmation is required. Follow-up kinematic and variability studies will provide further constraints on the properties of the newly detected groups/clusters of RSGs. The *V* band magnitudes of the newly discovered RSGs range from 13.7 mag to 17.2 mag, within the photometric and spectroscopic range covered by the upcoming mission Gaia.

*Acknowledgements.* This work was partially funded by the ERC Advanced Investigator Grant GLOSTAR (247078). The material in this work was partly supported by NASA under award NNG 05-GC37G, through the Long-Term Space Astrophysics program. This research was partly performed in the Rochester Imaging Detector Laboratory with support from a NYSTAR Faculty Development Program grant. Qingfeng Zhu thanks for the support by the Fundamental Research Funds for the Central Universities from Educational Department of China, #WK2030220001. MM and VI thank ESO for supporting a working visit of Dr. Ivanov at RIT. MM and ZQ acknowledge an awarded support from ESA/ESTEC to host Dr. Zhu. This publication makes use of data products from the Two Micron All Sky Survey, which is a joint project of the University of Massachusetts and the Infrared Processing and Analysis Center/California Institute of Technology, funded by the National Aeronautics and Space Administration and the National Science Foundation. This work is based [in part] on observations made with the Spitzer Space Telescope, which is operated by the Jet Propulsion Laboratory, California Institute of Technology under a contract with NASA. DENIS is the result of a joint effort involving human and financial contributions of several Institutes mostly located in Europe. It has been supported financially mainly by the French Institut National des Sciences de l'Univers, CNRS, and French Education Ministry, the European Southern Observatory, the State of Baden-Wuerttemberg, and the European Commission under a network of the Human Capital and Mobility program. This research made use of data products from the Midcourse Space Experiment, the processing of which was funded by the Ballistic Missile Defence Organization with additional support from the NASA office of Space Science. This research has made use of the SIMBAD data base, operated at CDS, Strasbourg, France. This publication makes use of data products from WISE, which is a joint project of the University of California, Los Angeles, and the Jet Propulsion Laboratory/California Insti- tute of Technology, funded by the National Aeronautics and Space Administration. We are thankful to the UKIRT team and SofI team for a great support during the observing runs, to the UKIDSS team in Cambridge for providing detailed information on the pipeline products, and to Dr. Stetson for providing the Daophot code, and helping with the installation. MM thanks Harm Habing and Ed Churchwell for discussions on GLIMPSE data, and J. Borissova, R. Kurtev, Saurabh Sharma, and G. R. Ivanov for discussions on stellar overdensities. MM is grateful to Jos de Bruine and Timo Prusti for useful discussions and support during her ESA fellowship. We thank the referee Ignacio Negueruela for his careful reading of our manuscript.

## References

Alard, C., Blommaert, J. A. D. L., Cesarsky, C., et al. 2001, ApJ, 552, 289
Alvarez, R., Lançon, A., Plez, B., & Wood, P. R. 2000, A&A, 353, 322
Alves, D. R. 2000, ApJ, 539, 732
Babusiaux, C. & Gilmore, G. 2005, MNRAS, 358, 1309
Benjamin, R. A., Churchwell, E., Babler, B. L., et al. 2003, PASP, 115, 953
Benson, P. J., Little-Marenin, I. R., Woods, T. C., et al. 1990, ApJS, 74, 911
Bessell, M. S., Castelli, F., & Plez, B. 1998, A&A, 333, 231
Bibby, J. L., Crowther, P. A., Furness, J. P., & Clark, J. S. 2008, MNRAS, 386, L23
Blum, R. D., Ramírez, S. V., Sellgren, K., & Olsen, K. 2003, ApJ, 597, 323
Borissova, J., Bonatto, C., Kurtev, R., et al. 2011, A&A, 532, A131
Borissova, J., Kumar, M. S. N., Amigo, P., et al. 2014, AJ, 147, 18
Buta, R. 1995, ApJS, 96, 39
Cabrera-Lavers, A., González-Fernández, C., Garzón, F., Hammersley, P. L., & López-Corredoira, M. 2008, A&A, 491, 781
Carpenter, J. M. 2001, AJ, 121, 2851
Chené, A.-N., Borissova, J., Bonatto, C., et al. 2013, A&A, 549, A98
Clampitt, L. & Burstein, D. 1997, AJ, 114, 699
Clark, J. S., Negueruela, I., Davies, B., et al. 2009, A&A, 498, 109
Comerón, F., Torra, J., Chiappini, C., et al. 2004, A&A, 425, 489
Cordes, J. M. & Lazio, T. J. W. 2002, Astrophysics e-prints: astro-ph/0207156

Davies, B., de La Fuente, D., Najarro, F., et al. 2012, MNRAS, 419, 1860
Davies, B., Figer, D. F., Kudritzki, R.-P., et al. 2007, ApJ, 671, 781
de Vaucouleurs, G. 1964, in IAU Symposium, Vol. 20, The Galaxy and the Magellanic Clouds, ed. F. J. Kerr, 88
de Wit, W. J., Testi, L., Palla, F., & Zinnecker, H. 2005, A&A, 437, 247
Drimmel, R., Cabrera-Lavers, A., & López-Corredoira, M. 2003, A&A, 409, 205
Drimmel, R. & Spergel, D. N. 2001, ApJ, 556, 181
Dutra, C. M., Bica, E., Soares, J., & Barbuy, B. 2003, A&A, 400, 533
Dutra, C. M., Santiago, B. X., & Bica, E. 2002, A&A, 381, 219
Egan, M. P., Price, S. D., Kraemer, K. E., et al. 2003, VizieR Online Data Catalog, 5114, 0
Ekström, S., Georgy, C., Eggenberger, P., et al. 2012, A&A, 537, A146
Epchtein, N., Deul, E., Derriere, S., et al. 1999, VizieR Online Data Catalog, 1, 2002
Fazio, G. G., Hora, J. L., Allen, L. E., et al. 2004, ApJS, 154, 10
Ferraro, F. R., Fusi Pecci, F., Testa, V., et al. 1995, MNRAS, 272, 391
Figer, D. F., MacKenty, J. W., Robberto, M., et al. 2006, ApJ, 643, 1166
Froebrich, D., Scholz, A., & Raftery, C. L. 2007, MNRAS, 374, 399
Frogel, J. A. & Whitford, A. E. 1987, ApJ, 320, 199
Glass, I. S., Whitelock, P. A., Catchpole, R. M., & Feast, M. W. 1995, MNRAS, 273, 383
Gonzalez, O. A., Rejkuba, M., Zoccali, M., Valenti, E., & Minniti, D. 2011, A&A, 534, A3
Gonzalez, O. A., Rejkuba, M., Zoccali, M., et al. 2012, A&A, 543, A13
González-Fernández, C. & Negueruela, I. 2012, A&A, 539, A100
Groenewegen, M. A. T. 2008, A&A, 488, 935
Groenewegen, M. A. T., Sloan, G. C., Soszyński, I., & Petersen, E. A. 2009, A&A, 506, 1277
Habing, H. J. & Olofsson, H., eds. 2003, Asymptotic giant branch stars. Astronomy and astrophysics library, New York, Berlin: Springer. Chapter 2 by Lattanzio, J.C. & Wood, P.R.
Habing, H. J., Sevenster, M. N., Messineo, M., van de Ven, G., & Kuijken, K. 2006, A&A, 458, 151
Hanson, M. M., Conti, P. S., & Rieke, M. J. 1996, ApJS, 107, 281
Hanson, M. M., Rieke, G. H., & Luhman, K. L. 1998, AJ, 116, 1915
Hodgkin, S. T., Irwin, M. J., Hewett, P. C., & Warren, S. J. 2009, MNRAS, 394, 675
Houk, N. & Smith-Moore, M. 1988, Michigan Catalogue of Two-dimensional Spectral Types for the HD Stars. Volume 4, Declinations $-26^{\circ}.0$ to $-12^{\circ}.0$.
Humphreys, R. M. & McElroy, D. B. 1984, ApJ, 284, 565
Ivanov, V. D., Borissova, J., Pessev, P., Ivanov, G. R., & Kurtev, R. 2002, A&A, 394, L1
Ivanov, V. D., Messineo, M., Zhu, Q., et al. 2010, in IAU Symposium, Vol. 266, IAU Symposium, ed. R. de Grijs & J. R. D. Lépine, 203–210
Ivanov, V. D., Rieke, M. J., Engelbracht, C. W., et al. 2004, ApJS, 151, 387
Kleinmann, S. G. & Hall, D. N. B. 1986, ApJS, 62, 501
Koornneef, J. 1983, A&A, 128, 84
Lancon, A. & Rocca-Volmerange, B. 1992, A&AS, 96, 593
Lejeune, T. & Schaerer, D. 2001, A&A, 366, 538
Levesque, E. M., Massey, P., Olsen, K. A. G., et al. 2005, ApJ, 628, 973
Lucas, P. W., Hoare, M. G., Longmore, A., et al. 2008, MNRAS, 391, 136
Marigo, P. 2001, A&A, 370, 194
Marigo, P., Girardi, L., Bressan, A., et al. 2008, A&A, 482, 883
Matsuura, M., Yamamura, I., Cami, J., Onaka, T., & Murakami, H. 2002, A&A, 383, 972
Mercer, E. P., Clemens, D. P., Meade, M. R., et al. 2005, ApJ, 635, 560
Messineo, M. 2004, PhD thesis, Leiden Observatory, Leiden University, P.O. Box 9513, 2300 RA Leiden, The Netherlands
Messineo, M., Davies, B., Figer, D. F., et al. 2011, ApJ, 733, 41
Messineo, M., Davies, B., Ivanov, V. D., et al. 2009, ApJ, 697, 701
Messineo, M., Habing, H. J., Menten, K. M., Omont, A., & Sjouwerman, L. O. 2004, A&A, 418, 103
Messineo, M., Habing, H. J., Menten, K. M., et al. 2005, A&A, 435, 575
Messineo, M., Menten, K. M., Churchwell, E., & Habing, H. 2012, A&A, 537, A10
Messineo, M., Menten, K. M., Figer, D., et al. 2014, ArXiv e-prints 1404.7297
Moorwood, A., Cuby, J.-G., & Lidman, C. 1998, The Messenger, 91, 9
Negueruela, I., González-Fernández, C., Marco, A., & Clark, J. S. 2011, A&A, 528, A59
Negueruela, I., González-Fernández, C., Marco, A., Clark, J. S., & Martínez-Núñez, S. 2010, A&A, 513, A74
Ortiz, R., Blommaert, J. A. D. L., Copet, E., et al. 2002, A&A, 388, 279
Paczyński, B. 1971, Acta Astron., 21, 417
Pietrinferni, A., Cassisi, S., Salaris, M., & Castelli, F. 2004, ApJ, 612, 168
Ramsay Howat, S. K., Ettedgui-Atad, E., Bennett, R. J., et al. 1998, in Society of Photo-Optical Instrumentation Engineers (SPIE) Conference Series, Vol. 3354, Society of Photo-Optical Instrumentation Engineers (SPIE) Conference Series, ed. A. M. Fowler, 456–467
Rayner, J. T., Cushing, M. C., & Vacca, W. D. 2009, ApJS, 185, 289
Rieke, G. H. & Lebofsky, M. J. 1985, ApJ, 288, 618
Schultheis, M., Ganesh, S., Glass, I. S., et al. 2000, A&A, 362, 215
Skrutskie, M. F., Cutri, R. M., Stiening, R., et al. 2006, AJ, 131, 1163
Soto, M., Barbá, R., Gunthardt, G., et al. 2013, A&A, 552, A101
Stetson, P. B. 1987, PASP, 99, 191
Vassiliadis, E. & Wood, P. R. 1993, ApJ, 413, 641
Wainscoat, R. J., Cohen, M., Volk, K., Walker, H. J., & Schwartz, D. E. 1992, ApJS, 83, 111
Wallace, L. & Hinkle, K. 1996, ApJS, 107, 312
Wegner, W. 1994, MNRAS, 270, 229
Wood, P. R., Bessell, M. S., & Fox, M. W. 1983, ApJ, 272, 99
Wright, E. L., Eisenhardt, P. R. M., Mainzer, A. K., et al. 2010, AJ, 140, 1868
Yang, M. & Jiang, B. W. 2011, ApJ, 727, 53
Zacharias, N., Monet, D. G., Levine, S. E., et al. 2004, in Bulletin of the American Astronomical Society, Vol. 36, American Astronomical Society Meeting Abstracts, 1418